Interaction Notes
Note 201
April 1973

An Integral-Equation Solution for TE Radiation and Scattering from Conducting Cylinders

J. H. Richmond
Ohio State University

ABSTRACT

The piecewise-sinusoidal reaction technique is applied to low frequency radiation and scattering from noncircular cylinders with perfect or imperfect conductivity. This report presents the theory, computer programs and numerical results for these two-dimensional problems with the TE polarization.

CONTENTS

I. INTRODUCTION

Low-frequency solutions for noncircular conducting cylinders have been presented in several published papers[1,2,3,4,5,6,7,8]. Point-matching procedures were employed by Mei and Van Bladel[1], Andreasen[2] and Wallenberg and Harrington[5]. In the point-matching technique, the contour of the cylinder is divided into segments and the integral equation is enforced at the center of each segment.

Mei and Van Bladel used rectangular pulses as basis functions for expanding the surface-current density. They employed trapezoidal-rule integration, sampling the integrand only at the center of each segment. Andreasen used Simpson's-rule integration and a piecewise-parabolic expansion for the current. Wallenberg and Harrington used a second-order polynomial for the expansion functions, with discontinuities in the current density at the endpoints of each segment.

In this report, Rumsey's reaction concept[9] is employed to formulate an integral-equation solution for radiation and scattering from cylinders with perfect or imperfect conductivity. A piecewise-sinusoidal expansion is employed for the current distribution on the conducting surface. The complex coefficients in this expansion represent samples of the current function. The unknown current distribution is forced to have the correct reactions with sinusoidal electric test sources located on the conducting surface. (Since the test functions are the same as the expansion functions, this is an application of Galerkin's method[10].) This procedure generates a system of simultaneous linear equations. Numerical solution of this system yields a stationary result for the samples of the current distribution. Finally the admittance, gain, far-field pattern and echo width are determined from the current distribution.

The new solution appears to be advantageous with respect to computational efficiency, convergence, accuracy and generality. The current distribution is represented by a continuous function, the impedance matrix is symmetric, and the solution satisfies the reciprocity and forward-scattering theorems.

This report considers two-dimensional electromagnetic problems involving infinitely-long conducting cylinders. We are concerned with the time-harmonic TE case where the field has no z-dependence, E_z vanishes everywhere, and the time dependence $e^{j\omega t}$ is understood and suppressed. (The z axis is parallel with the axis of the cylinder.) With no significant loss of generality, we restrict our attention to polygon cylinders. The surrounding medium is free space. The source may be an incident plane wave, a parallel magnetic line-source near the cylinder, or an axial-slot aperture on the surface of the cylinder.

With perfect conductivity, the computer programs will handle open as well as closed cylinders, arrays of cylinders, and interior as well as exterior sources. With finite conductivity, however, the programs are restricted to closed cylinders.

The remaining text presents the detailed theory and some numerical results, and the computer programs are listed in the Appendices.

II. THE REACTION TECHNIQUE

The reaction concept and its applications have been discussed by Rumsey[9], Cohen[11], Harrington[12] and Richmond[13].

Consider the exterior scattering problem illustrated in Fig. 1a. (Radiation problems and open surfaces are discussed later.) In the presence of a dielectric or conducting body, the impressed electric and magnetic currents $(\underline{J}_i, \underline{M}_i)$ generate the electric and magnetic field intensities $(\underline{E}, \underline{H})$. For simplicity, let the exterior medium be free space.

From the surface-equivalence theorem of Schelkunoff[14], the interior field will vanish (without disturbing the exterior field) if we introduce the following surface-current densities

$$\underline{J}_s = \hat{n} \times \underline{H} \tag{1}$$

$$\underline{M}_s = \underline{E} \times \hat{n} \tag{2}$$

on the closed surface S of the scatterer. (The unit vector $\hat{n}$ is directed outward on S.) In this situation, illustrated in Fig. 1b, we may replace the scatterer with free space without disturbing the field anywhere.

By definition, the incident field $(\underline{E}_i, \underline{H}_i)$ is generated by $(\underline{J}_i, \underline{M}_i)$ in free space, and the scattered field is:

$$\underline{E}_s = \underline{E} - \underline{E}_i \tag{3}$$

$$\underline{H}_s = \underline{H} - \underline{H}_i \quad . \tag{4}$$

When the surface current $(\underline{J}_s, \underline{M}_s)$ radiates in free space, it generates the field $(\underline{E}_s, \underline{H}_s)$ in the exterior and $(-\underline{E}_i, -\underline{H}_i)$ in the interior region. This result, illustrated in Fig. 1c, is deduced from Fig. 1b and the superposition theorem.

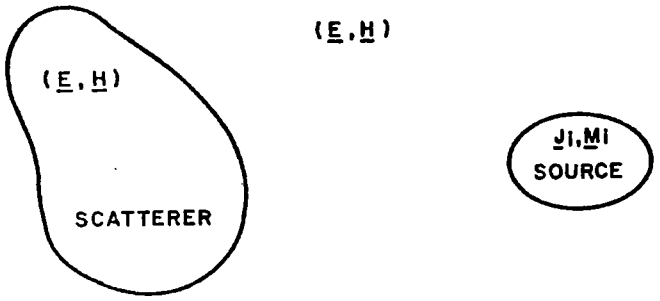

Fig. 1a. The source $(\underline{J}_i, \underline{M}_i)$ generates the field $(\underline{E}, \underline{H})$ with scatterer.

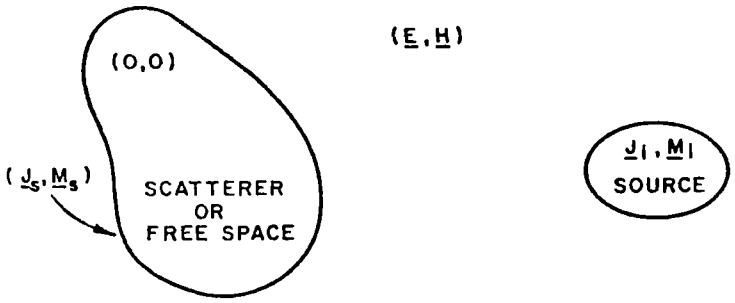

Fig. 1b. The interior field vanishes when the currents $(\underline{J}_S, \underline{M}_S)$ are introduced on the surface of the scatterer.

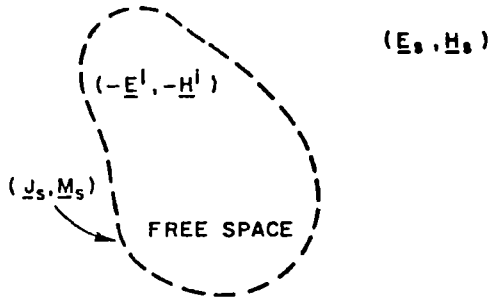

Fig. 1c. The exterior scattered field may be generated by $(\underline{J}_S, \underline{M}_S)$ in free space.

With the scatterer replaced by free space, we have noted in Fig. 1b that the interior region has a null field. As shown in Fig. 2, we place an electric test source $\underline{J}_t$ in this region and find from the reciprocity theorem that

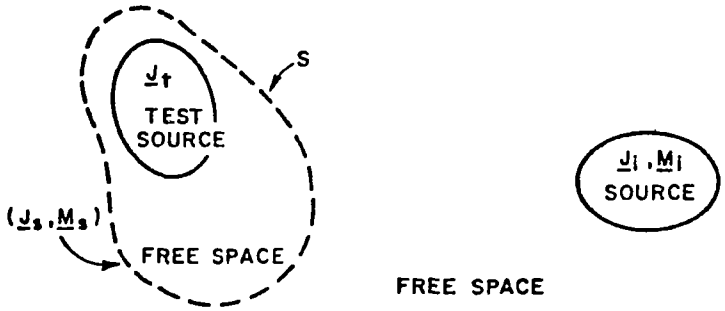

Fig. 2. An electric test source $\underline{J}_t$ is positioned in the interior of the scattering region.

$$(5) \qquad \oiint_S (\underline{J}_s \cdot \underline{E}_t - \underline{M}_s \cdot \underline{H}_t)\, ds + \iiint (\underline{J}_i \cdot \underline{E}_t - \underline{M}_i \cdot \underline{H}_t)\, dv = 0$$

where $(\underline{E}_t, \underline{H}_t)$ is the free-space field of the test source. In words, Eq. (5) states that the interior test source has zero reaction with the other sources. This "zero-reaction theorem" was developed by Rumsey[9].

Equation (5) is the integral equation for the scattering problem, and our objective is to use this equation to determine the surface-current distributions $\underline{J}_s$ and $\underline{M}_s$. To accomplish this, we expand these functions in finite series so there will be a finite number N of unknown expansion constants. Next we obtain N simultaneous linear equations to permit a solution for these constants. One such equation is obtained from Eq. (5) each time we set up a new test source.

The magnetic current $\underline{M}_s$ vanishes if the scatterer is a perfect conductor. We assume a finite conductivity and use the impedance boundary condition:

$$(6) \qquad \underline{M}_s = Z_s \, \underline{J}_s \times \hat{n}$$

where Z_s denotes the surface impedance.

For two-dimensional problems involving cylindrical scatterers, $\underline{J}_s$ and $\underline{M}_s$ are functions only of the position ℓ around the contour C of the cylinder. If $\underline{J}_i$ vanishes, Eqs. (5) and (6) yield

$$(7) \qquad \oint_C \underline{J}_s \cdot [\underline{E}_m - (\hat{n} \times \underline{H}_m) Z_s] \, d\ell = \iint \underline{M}_i \cdot \underline{H}_m \, ds$$

where $(\underline{E}_m, \underline{H}_m)$ denotes the free-space field of test-source m.

We represent the electric current distribution as follows:

$$(8) \qquad \underline{J}_s(\ell) = \sum_{n=1}^{N} I_n \, \underline{J}_n(\ell)$$

where the complex constants I_n are samples of the function $J_s(\ell)$. The vector functions $\underline{J}_n(\ell)$ are known as basis functions, subsectional bases, expansion functions or dipole modes. We employ expansion functions $\underline{J}_n$ and test sources $\underline{J}_m$ with unit current density at their terminals.

From Eqs. (7) and (8) we obtain the simultaneous linear equations

$$(9) \qquad \sum_{n=1}^{N} I_n \, Z_{mn} = V_m \qquad \text{with } m = 1, 2, 3, \cdots N$$

where

$$(10) \qquad Z_{mn} = - \int_n \underline{J}_n(\ell) \cdot [\underline{E}_m - (\hat{n} \times \underline{H}_m) Z_s] \, d\ell = - \int_m \underline{J}_m(\ell) \cdot \underline{E}_n \, d\ell$$

$$(11) \qquad V_m = - \iint_i \underline{M}_i \cdot \underline{H}_m \, ds = \int_m \underline{J}_m \cdot \underline{E}_i \, d\ell \quad .$$

In Eqs. (10) and (11) the integrations extend over the region where the integrand is non-zero. For example, region n is that portion of the contour C covered by the expansion function $\underline{J}_n$. Region m covers the interior test source $\underline{J}_m$. The reciprocity theorem relates the first and second integrals in Eq. (10). In the second integral, $\underline{E}_n$ is the free-space field generated by $\underline{J}_n$ and the associated magnetic current $\underline{M}_n$.

For computational speed and storage, it will be advantageous to have a symmetric impedance matrix Z_{mn}. Furthermore, the test sources should be selected to yield a well-conditioned set of simultaneous linear equations. For these reasons and to obtain closed forms for some of the integrals in Eqs. (10) and (11), we employ test sources $\underline{J}_m$ of the same size, shape and functional form as the expansion functions $\underline{J}_n$. Finally, we position the interior test sources a small distance δ from surface S and take the limiting form of the integrals as δ tends to zero.

In this section we have considered explicitely the exterior scattering problem. With a slight change in wording, we could make the discussion apply equally well to the interior scattering problem. To accomplish this, replace "interior region" with "source-free region" and replace "exterior region" with "source region". Thus, the unit vector $\hat{n}$ is directed into the source region (which contains $\underline{M}_i$), and we let the test sources approach surface S from the source-free region.

The next two sections discuss the electric strip dipoles which are employed as test sources and expansion modes. Since each dipole is comprised of two strip monopoles, the monopoles are considered first.

III. TRANSVERSE-ELECTRIC STRIP MONOPOLES

Consider the "strip monopole" illustrated in Fig. 3. This

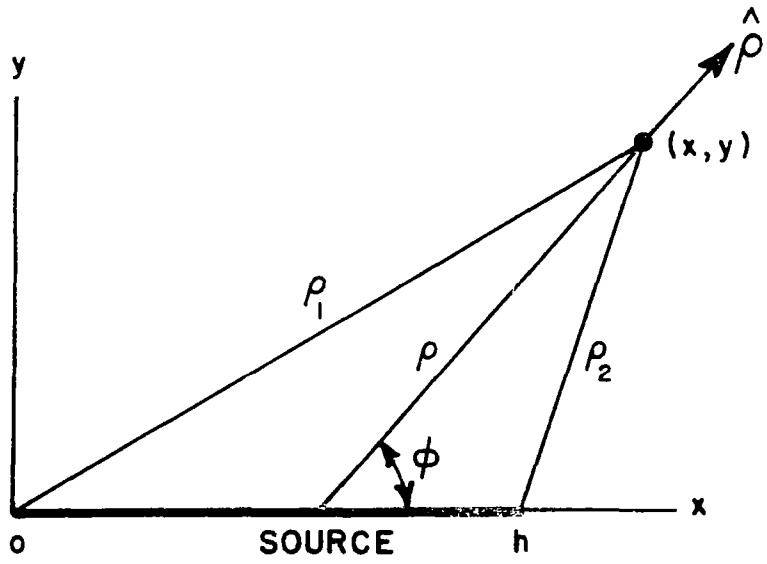

Fig. 3. An electric strip monopole and the coordinate system.

source is an electric surface-current density $\underline{J} = \hat{x}\, J(x)$ located on the xz plane. The source has width h and infinite length and radiates in free space. By superposition, the scattered field of a perfectly conducting polygon cylinder may be regarded as the field of an array of strip monopoles. For the strip monopole shown in Fig. 3, the potentials and fields are:

$$\underline{A} = -\frac{j\mu}{4} \int_0^h \underline{J}\, H_0(k\rho)\, dx' \tag{12}$$

$$V = \frac{1}{4\omega\varepsilon} \int_0^h J'\, H_0(k\rho)\, dx' \tag{13}$$

$$E_x = -\frac{k\eta}{8} \int_0^h J[H_0(k\rho) + H_2(k\rho)\cos(2\phi)]\, dx' \tag{14}$$

$$E_y = -\frac{k\eta}{8} \int_0^h J\, H_2(k\rho)\sin(2\phi)\, dx' \tag{15}$$

$$\underline{H} = -\frac{jk}{4} \int_0^h \underline{J} \times \hat{\rho}\, H_1(k\rho)\, dx' \tag{16}$$

where

$$\rho = \sqrt{(x - x')^2 + y^2} \tag{17}$$

$$k = \omega\sqrt{\mu\varepsilon} \tag{18}$$

$$\eta = \sqrt{\mu/\varepsilon} \tag{19}$$

$$J' = \frac{dJ}{dx'} \tag{20}$$

and the superscript (2) is understood on the Hankel functions H_0, H_1 and H_2. A useful alternative form for the electric field is

$$\underline{E} = -j\omega\underline{A} - \nabla V \tag{21}$$

$$(22) \qquad \underline{E} = -\frac{k\eta}{4} \int_0^h \underline{J}\, H_0(k\rho)\, dx' + \frac{\eta}{4} \int_0^h \hat{\rho}\, J'\, H_1(k\rho)\, dx' \quad .$$

For most current functions J(x), the field integrals must be evaluated with infinite-series expansions or numerical integration procedures. For the sinusoidal current distribution, however, E_x is obtained rigorously in simple closed form. Thus, if

$$(23) \qquad \underline{J}(x) = \hat{x}\, [I_1 \sin(kh - kx) + I_2 \sin(kx)] \,/\, \sin(kh)$$

then

$$(24) \qquad E_x = \frac{\eta}{4 \sin(kh)} [I_1 H_0(k\rho_1) \cos(kh) - I_1 H_0(k\rho_2) + I_2 H_0(k\rho_2) \cos(kh) - I_2 H_0(k\rho_1)]$$

where I_1 and I_2 represent J(x) at x = 0 and x = h, respectively. The current distribution in Eq. (23) implies line charges at the edges of the strip monopole. Since our model of the polygon cylinder will have no line charges, the line-charge field contributions are not included in Eq. (24). We obtained Eq. (24) by integrating the field of the sinusoidal electric line source. Unfortunately, the integral for E_y must be evaluated by numerical methods.

IV. THE SINUSOIDAL STRIP DIPOLE

A planar strip dipole is illustrated in Fig. 4a. This dipole lies in the xz plane and has infinite length in the z direction. The surface-current density is

$$(25) \qquad \underline{J} = \hat{x}\, \frac{\sin k(x - x_1)}{\sin k(x_2 - x_1)} \qquad \text{for} \quad x_1 < x < x_2$$

$$(26) \qquad \underline{J} = \hat{x}\, \frac{\sin k(x_3 - x)}{\sin k(x_3 - x_2)} \qquad \text{for} \quad x_2 < x < x_3 \quad .$$

As indicated in Fig. 4b, the current density vanishes at the edges x_1 and x_3, is continuous across the terminals at x_2 and has a slope discontinuity at x_2.

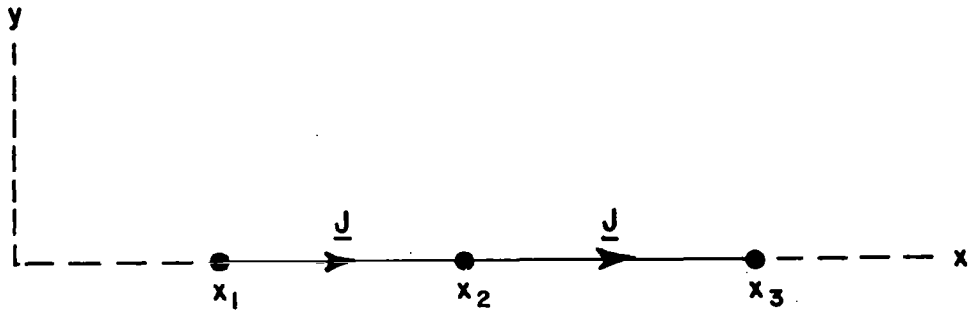

Fig. 4a. A planar strip dipole with edges at x_1 and x_3 and terminals at x_2.

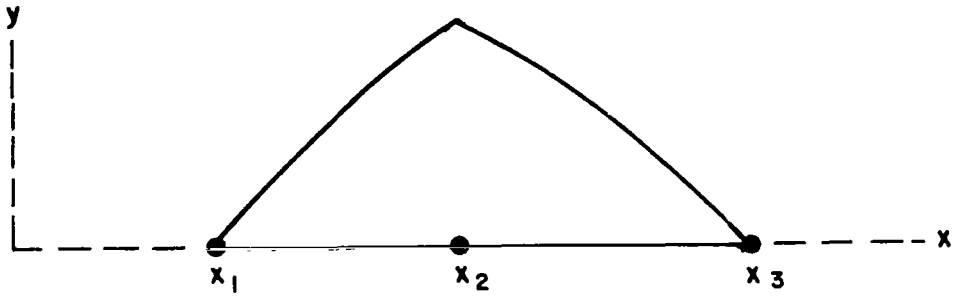

Fig. 4b. The current-density distribution $\underline{J}$ on the sinusoidal strip dipole.

The sinusoidal strip dipole is a hypothetical source in free space. The current distribution on a conducting strip is not sinusoidal.

Figure 5 illustrates a strip V-dipole. Distance along the dipole arms is measured by the coordinates s and t with origin at the terminals 0. The surface-current density is

$$\underline{J} = -\hat{s}\,\frac{\sin k(s_1 - s)}{\sin ks_1} \qquad \text{on arm s} \tag{27}$$

$$\underline{J} = \hat{t}\,\frac{\sin k(t_1 - t)}{\sin kt_1} \qquad \text{on arm t} \tag{28}$$

TABLE I

Self Impedance of Center-Fed Strip-Dipole Shown in Figure 5
$s_1 = t_1 = h$

ψ	$h/\lambda = 0.05$	$h/\lambda = 0.10$	$h/\lambda = 0.15$	$h/\lambda = 0.20$
45°	0.11 -j 14.1	0.47 -j 13.4	1.20 -j 12.2	2.53 -j 10.4
90°	0.38 -j 20.9	1.59 -j 19.3	3.94 -j 17.1	8.10 -j 14.0
135°	0.64 -j 24.3	2.68 -j 22.2	6.49 -j 19.5	12.95 -j 16.4
180°	0.75 -j 25.3	3.11 -j 23.0	7.50 -j 20.3	14.77 -j 17.4

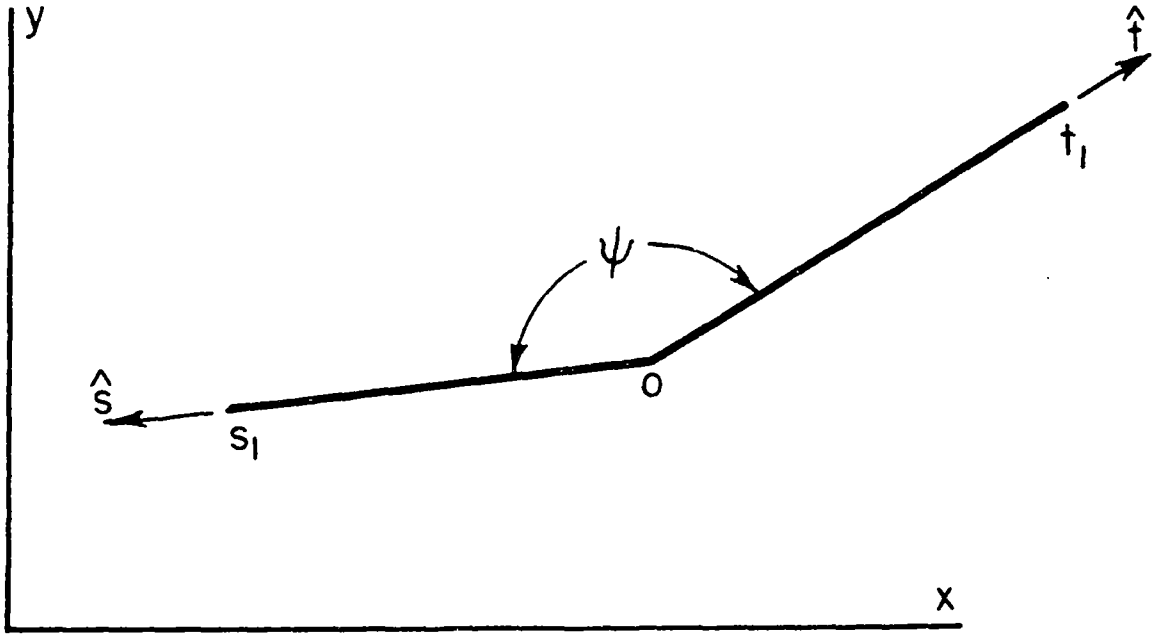

Fig. 5. Nonplanar strip dipole with edges at s_1 and t_1 and terminals at 0.

where the unit vectors $\hat{s}$ and $\hat{t}$ are perpendicular to the z axis. Thus, the current density vanishes at the edges s_1 and t_1 and has unit value at the terminals 0. The edges of the dipole are parallel with the z axis. If the wedge angle ψ is adjusted to 180 degrees, the V-dipole in Fig. 5 reduces to the planar dipole in Fig. 4.

Having defined the sinusoidal strip dipole, we are now in a position to explain its relevance. We shall use the dipole current distribution (Eqs. (27) and (28)) as the basis function ($\underline{J}_n$ in Eq.(8)) for expanding the unknown current distribution induced on a conducting cylinder. Furthermore, strip dipoles will be employed as test sources with the reaction concept to solve the integral equation.

By superposition, the field of the strip dipole in Fig. 5 is the sum of the field contributions from monopoles s and t. The field from each monopole can be calculated from Eqs. (12) through (24) with the appropriate coordinate transformations.

Although the sinusoidal strip dipole is a hypothetical source, it is useful to define its self impedance with the induced-emf formulation:

$$(29) \qquad Z = -\int_0^{s_1} \underline{J}(s)\cdot\underline{E}\, ds - \int_0^{t_1} \underline{J}(t)\cdot\underline{E}\, dt$$

where $\underline{J}(s)$ and $\underline{J}(t)$ are given by Eqs. (27) and (28) and $\underline{E}$ is the free-space field of the strip dipole. The reciprocal of Z yields the admittance per unit length of the strip dipole. Table I lists the self impedance of a center-fed sinusoidal strip dipole as a function of the angle ψ and the segment length $s_1 = t_1 = h$.

The mutual impedance between two strip dipoles is defined by

$$(30) \qquad Z_{12} = -\int_0^{s_1} \underline{J}_2(s)\cdot\underline{E}_1\, ds - \int_0^{t_1} \underline{J}_2(t)\cdot\underline{E}_1\, dt$$

where $\underline{J}_2(s)$ and $\underline{J}_2(t)$ are given by Eqs. (27) and (28) and $\underline{E}_1$ is the free-space field of the first dipole.

Figure 6 illustrates a pair of center-fed planar strip dipoles, and Table II lists their mutual impedance Z_{12}. Here ρ and ϕ specify the relative positions of the dipoles, β specifies the relative orientation, and each dipole has the same segment length h.

Table III lists the mutual impedance Z_{12} of the overlapping strip dipoles shown in Fig. 7. Each of the three segments has the same length h, dipoles 1 and 2 share the center segment, and the angles ψ are identical. Finally, Table IV gives the mutual impedance of the overlapping strip dipoles shown in Fig. 8. These dipoles share an end segment.

TABLE II

Mutual Impedance of Center-Fed Planar Strip-Dipoles Shown in Figure 6

Segment length: $h/\lambda = 0.1$
Distance between midpoints: $\rho/\lambda = 0.3$

ϕ	$\beta = 0$	$\beta = 45°$	$\beta = 90°$	$\beta = 135°$
0	1.94 +j 0.81	1.36 +j 0.39	0.00 +j 0.00	-1.36 -j 0.39
30°	1.42 -j 0.58	1.62 +j 1.07	0.87 +j 1.80	-0.38 +j 1.73
60°	0.39 -j 2.68	0.90 -j 0.66	0.87 +j 1.80	0.34 +j 3.03
90°	-.13 -j 3.53	-.08 -j 2.57	0.00 +j 0.00	0.08 +j 2.57

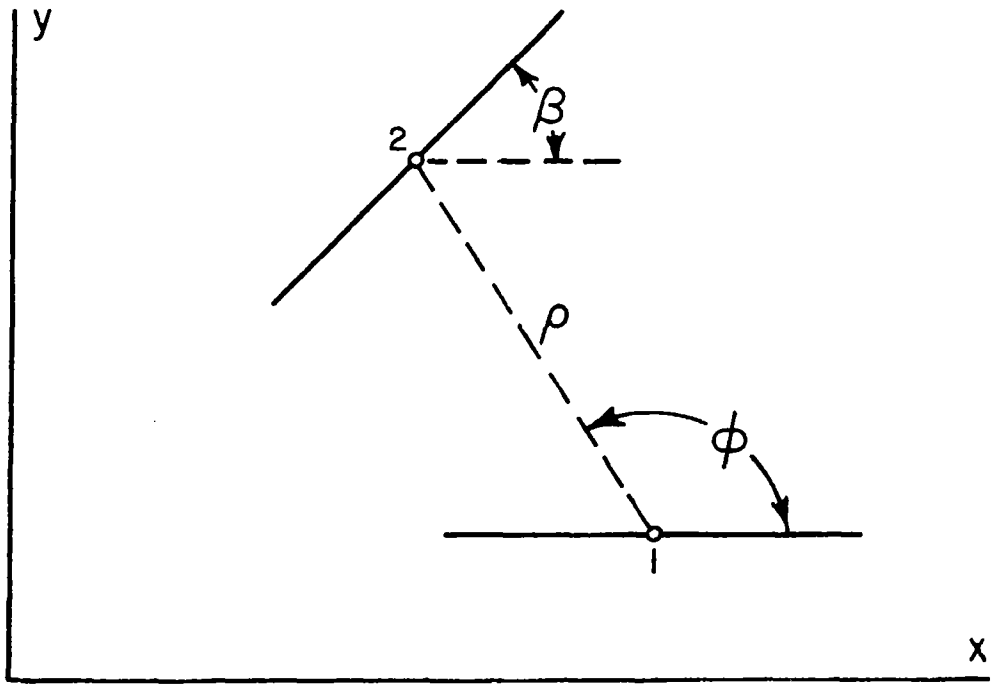

Fig. 6. Coupled strip dipoles.

TABLE III

Mutual Impedance of Center-Fed Overlapping Dipoles Shown in Figure 7

ψ	$h/\lambda = 0.05$	$h/\lambda = 0.10$	$h/\lambda = 0.15$	$h/\lambda = 0.20$
60°	-0.09 +j 8.89	-0.33 +j 9.85	-0.59 +j 11.9	-0.66 +j 15.9
90°	0.01 +j 6.99	0.14 +j 8.26	0.77 +j 10.8	2.64 +j 15.2
120°	0.29 +j 6.67	1.31 +j 8.22	3.52 +j 10.6	7.88 +j 13.9
150°	0.60 +j 6.65	2.49 +j 8.16	5.88 +j 9.8	11.29 +j 11.0
180°	0.74 +j 6.67	2.97 +j 8.10	6.73 +j 9.2	12.23 +j 9.6

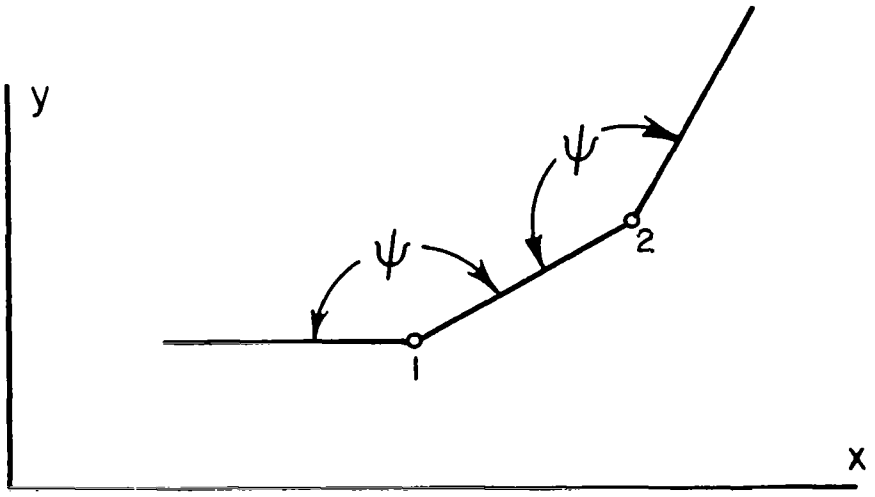

Fig. 7. Overlapping strip dipoles share the center segment.

TABLE IV

Mutual Impedance of Center-Fed Overlapping Dipoles Shown in Figure 8

α	$h/\lambda = 0.05$	$h/\lambda = 0.10$	$h/\lambda = 0.15$	$h/\lambda = 0.20$
30°	0.60 -j 16.4	2.51 -j 14.7	6.03 -j 12.8	11.83 -j 11.0
60°	0.28 -j 11.7	1.18 -j 10.7	2.88 -j 9.43	5.80 -j 7.84
90°	0.00 -j 8.25	0.04 -j 7.82	0.20 -j 6.93	0.71 -j 5.29
120°	-0.09 -j 5.17	-0.38 -j 5.14	-0.86 -j 4.84	-1.56 -j 3.99
150°	-0.04 -j 2.21	-0.18 -j 2.32	-0.46 -j 2.43	-0.94 -j 2.50

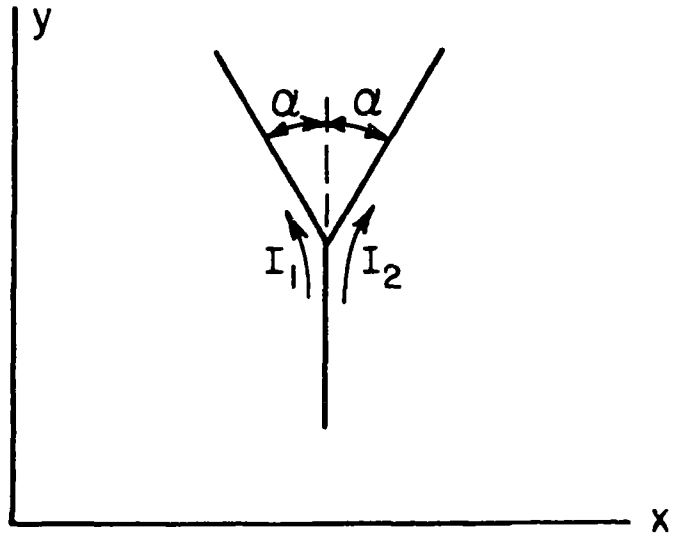

Fig. 8. Dipoles 1 and 2 share one segment in a Y configuration.

V. CYLINDERS WITH PERFECT CONDUCTIVITY

Consider a perfectly conducting polygon cylinder with contour C which may be open or closed. Let $J_s(\ell)$ denote the surface-current density induced on the cylinder. If the cylinder is closed, J_s will flow entirely on the outside or inside of surface S in accordance with the location of the source. If the cylinder is open, currents will flow on both sides of the thin conducting surface. In all cases, we let J_s denote the total current density.

Figure 9a illustrates a perfectly conducting polygon cylinder illuminated by a parallel magnetic line source M_i. Let I_1 and I_2 denote the current density J_s at the corners of the polygon. The current J_s vanishes at the edges 0 and 0'. Let us define two strip-dipole mode currents on the cylinder. Mode 1 extends from point 0 to point 2 and has terminals at point 1. Mode 2 extends from 1 to 3 with terminals at 2. Each mode has a sinusoidal current distribution and unit terminal current as in Eqs. (27) and (28). Now we represent $J_s(\ell)$ as the superposition of the two modal currents with weightings I_1 and I_2. This gives a piecewise-sinusoidal expansion for $J_s(\ell)$ with two unknown constants I_1 and I_2. (In practice we require a minimum of around 16 unknowns to obtain accurate results.)

In the exact solution, the tangential electric field vanishes everywhere on contour C. Thus if we move an electric test probe to the conducting surface, as in Fig. 9b, the open-circuit voltage at its terminals will read zero. To determine N current samples, we make N independent probing tests. The probes may be real (thin-wire V-dipoles) or hypothetical (electric line sources or strip dipoles). Now suppose we adjust the currents I_n until all the probes read zero. This procedure yields a stationary solution for the currents I_n and, under favorable conditions, tends to the rigorous solution as N increases.

Let Z_{mn} denote the mutual impedance between test-probe m in Fig. 9b and mode current n in Fig. 9a. The open-circuit voltage induced in the probe is the sum of the voltage contributions from J_s and M_i. This voltage must vanish at each probe, leading again to Eqs. (9) and (11). With strip-dipole probes, Z_{mn} is given by Eq. (29) and Table I for the diagonal elements and by Eq. (30) and Tables II, III and IV for the off-diagonal elements. For perfectly conducting cylinders, the impedance matrix is symmetric.

Our piecewise-sinusoidal expansion for the current density $J_s(\ell)$ satisfies Kirchoff's current law. This follows from the continuous nature of each dipole mode in the expansion. In this respect, our mode currents resemble the loop currents (as opposed to branch currents) in electric circuits.

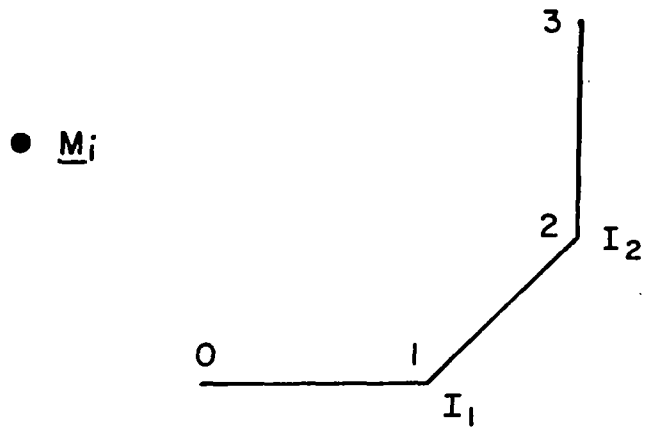

Fig. 9a. Perfectly conducting polygon cylinder with parallel magnetic line source $\underline{M}_i$.

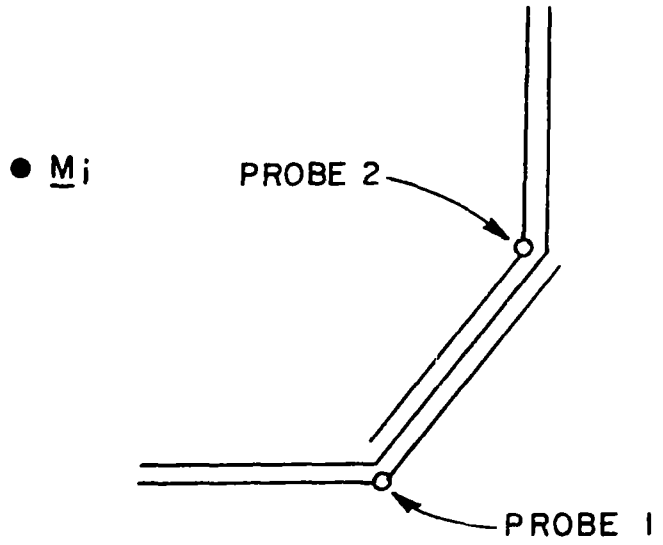

Fig. 9b. Electric test probes 1 and 2 are moved to the conducting surface.

Figure 10 shows a square cylinder with a fin extending outward

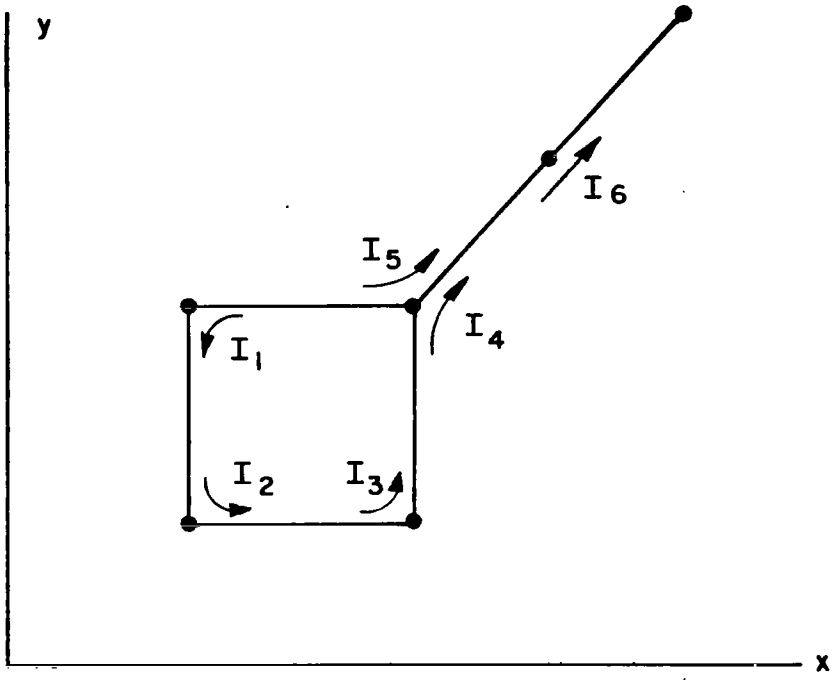

Fig. 10. Perfectly conducting cylinder illustrates first, second and third-order junctions.

from one corner. This illustrates first, second and third-order junctions. (The order of a junction is defined by the number of strips extending outward from the junction.) In Fig. 10 the open edge of the fin is a first-order junction. Second-order junctions exist at the terminals of modes I_1, I_2, I_3 and I_6. The upper-right corner of the square cylinder is a third-order junction. At a junction of order n, it is possible to define at least n distinct modes. As a consequence of Kirchoff's current law, however, only (n - 1) modes are independent.

In Fig. 10 the current density I_4 flows into the third-order junction from below, I_5 into it from the left, and $(I_4 + I_5)$ flows out of the junction via the fin.

As illustrated in Fig. 10, a planar conducting surface is sometimes divided into two or more segments. The absolute upper limit on segment length is $\lambda/2$. For accurate results, however, we must use at least four segments per wavelength.

VI. CYLINDERS WITH FINITE CONDUCTIVITY

Section II presents the reaction formulation for closed cylinders with finite conductivity. Although the impedance matrix Z_{mn} is symmetric for perfectly conducting cylinders, the symmetry disappears with finite conductivity. In the square matrix Z_{mn}, the first subscript m denotes the row and the second subscript n denotes the column. In the linear equations (Eq. (9)), equation m is obtained by enforcing the zero-reaction condition with test source m. In Eq. (10), Z_{mn} is the mutual impedance between the test source (or test probe) m and the expansion mode n. The test sources and the expansion modes are electric strip dipoles. With finite conductivity, however, the electric expansion modes have associated magnetic currents given by Eq. (6).

In Eq. (10), the unit normal vector $\hat{n}$ is directed into the source region. By definition, the source region contains the impressed current $\underline{M}_i$. Thus $\hat{n}$ reverses direction if $\underline{M}_i$ is moved across the conducting surface S. For perfectly conducting cylinders, the impedance matrix Z_{mn} is independent of the source location. With finite conductivity, however, it is apparent in Eq. (10) that the interior matrix differs numerically from the exterior matrix.

The impedance boundary condition (Eq. (6)) is not rigorous but is a reasonable approximation when Z_s is small.

It may be noted from Eqs. (10) and (16) that the mutual impedance Z_{mn} between coplanar non-overlapping strip dipoles is independent of the surface impedance Z_s.

VII. THE EXCITATION COLUMN

The complex voltages V_m in Eq. (9) form the "excitation column" or "excitation vector" in the matrix equation $Z_{mn}\, I_n = V_m$. These voltages are independent of the surface impedance Z_s. If the impressed current is a magnetic line source $\underline{M}_i$, Eq. (11) reduces to

$$(31) \qquad V_m = \int_m \underline{J}_m \cdot \underline{E}_i \, d\ell = - \underline{M}_i \cdot \underline{H}_m \quad .$$

The two forms in Eq. (31) are related by the reciprocity theorem. Both forms require numerical integration over test source m.

If the line source $\underline{M}_i$ is located at a great distance from the cylinder, the incident field ($\underline{E}_i$, $\underline{H}_i$) may be regarded as a plane wave with

$$\underline{E}_i = - \hat{\phi}_i \, \eta \, H_o \, e^{jk(x \cos\phi_i + y \sin\phi_i)} \tag{32}$$

where ϕ_i is the angular coordinate of the source and H_o is the incident magnetic field intensity at the coordinate origin. Figure 11 illustrates

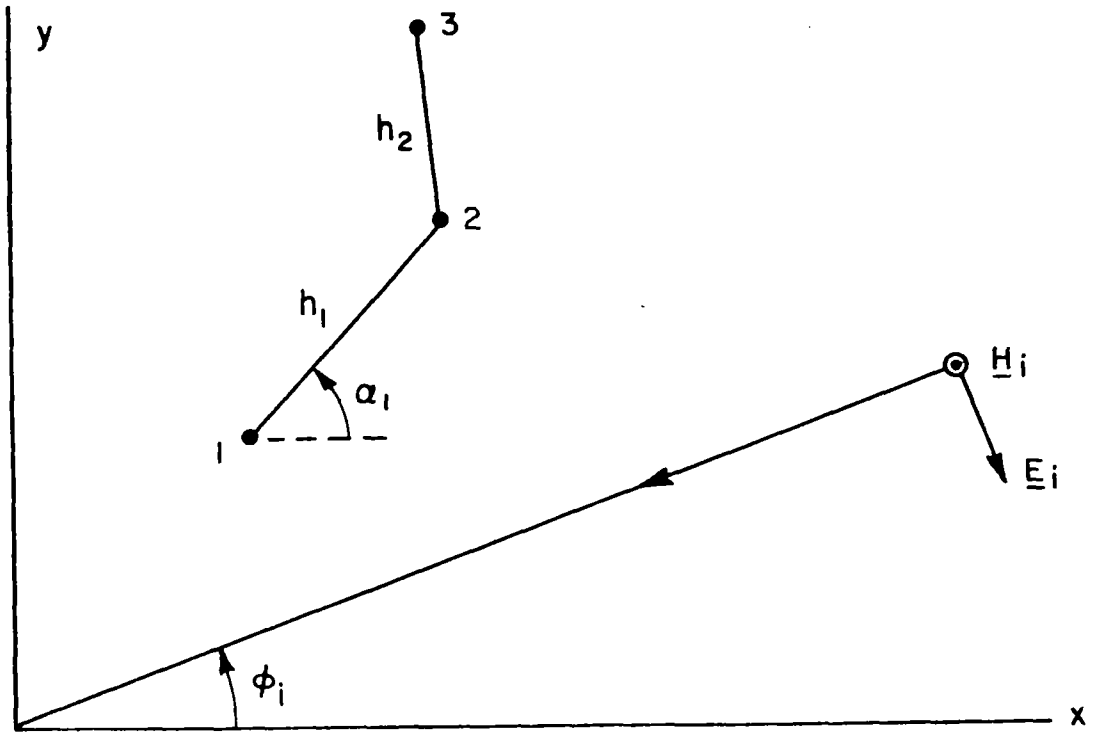

Fig. 11. A plane wave ($\underline{E}_i$, $\underline{H}_i$) illuminates an electric strip dipole.

an incident plane wave illuminating a strip dipole with edges at points 1 and 3 and terminals at point 2. Let the sinusoidal electric current $\underline{J}_m$ flow in the direction from 1 to 2 and from 2 to 3. The integration in Eq. (31) is readily performed to yield

$$V_m = - \eta H_o \frac{[e^{j\psi_1} - (\cos kh_1 - j \cos(\alpha_1 - \phi_i) \sin kh_1) e^{j\psi_2}]}{k \sin kh_1 \sin(\alpha_1 - \phi_i)} + \eta H_o \frac{[e^{j\psi_3} - (\cos kh_2 - j \cos(\alpha_2 - \phi_i) \sin kh_2) e^{j\psi_2}]}{k \sin kh_2 \sin(\alpha_2 - \phi_i)} \tag{33}$$

where h_1 and h_2 are the dipole segment lengths and $\psi_j = k(x_j \cos\phi_i + y_j \sin\phi_i)$. The angle between the positive x axis and the vector directed to the terminals from point 1 is denoted α_1. Similarly α_2 is the angle of the vector directed to the terminals from point 3.

To investigate the properties of a narrow axial slot in a cylinder, we move a magnetic line source $\underline{M}_j$ to the conducting surface. This situation is illustrated in Fig. 12 with the line source located

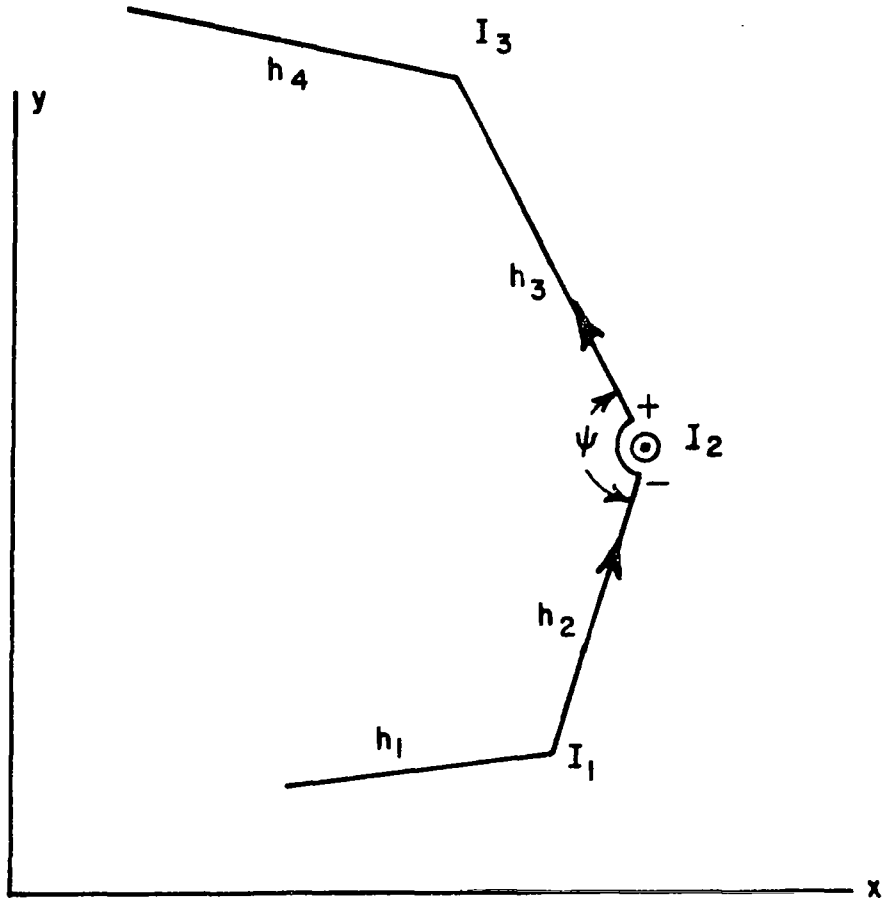

Fig. 12. A narrow axial slot is modeled with a magnetic line source at the conducting surface.

at the terminals of dipole mode I_2. The arrows on segments h_2 and h_3 indicate the reference directions for $\underline{J}_2$. The circled dot represents the magnetic line current $\underline{M}_i$ flowing in the positive z direction. The aperture voltage is M_i with reference polarity indicated by the positive and negative signs in Fig. 12.

To calculate the excitation column for this situation, we refer again to Eq. (31) and consider the limiting form of the integrals as $\underline{M}_i$ approaches the conducting cylinder from the right. Only the integrations over segments h_2 and h_3 require special attention; the others are amenable to numerical integration. We position the line source $\underline{M}_i$ at the intersection of segments h_2 and h_3. Thus the field $\underline{E}_i$ is orthogonal to the conducting surfaces h_2 and h_3 except on the circular-arc region with angle ψ. Since the mode current $\underline{J}_1$ goes sinusoidally to zero near the line source, V_1 requires integration only over h_1 with no contribution from h_2. Likewise V_3 is obtained by integrating over h_4 with no contribution from h_3. The mode current J_2 has unit value in the vicinity of the line source, and Eq. (31) yields in the limit (as the radius of arc ψ tends to zero)

$$V_2 = \frac{\psi M_i}{2\pi} \quad . \tag{34}$$

With aperture voltage M_i and aperture current I_2, the aperture admittance is

$$Y = I_2/M_i = G + j\,B \quad \text{mhos/meter.} \tag{35}$$

As the aperture width tends to zero, the susceptance B is singular. The conductance G, however, is well behaved and the time-average power delivered by the line source is

$$P = |M_i|^2\, G \quad \text{watts/meter.} \tag{36}$$

In Fig. 12, if the line source approaches the conducting surface from the left we find

$$V_2 = -\frac{(2\pi - \psi)\, M_i}{2\pi} \tag{37}$$

but the other excitation voltages are not affected. If the cylinder is closed, this change in one excitation voltage converts an antenna radiation problem to an interior cavity problem. For a perfectly conducting cylinder, the aperture conductance will be positive in the radiating case and zero in the cavity case. If $\psi = \pi$, moving the line source across the conducting wall simply reverses the sign of one voltage.

The slot discussed above is called a "one-sided slot" since it illuminates only the region on one side of the thin conducting wall. Figure 13a illustrates a one-sided axial slot and the line-source model.

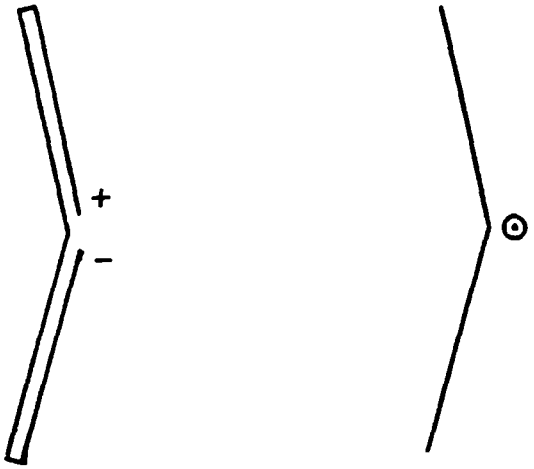

Fig. 13a. A one-sided slot is modeled with a magnetic line source.

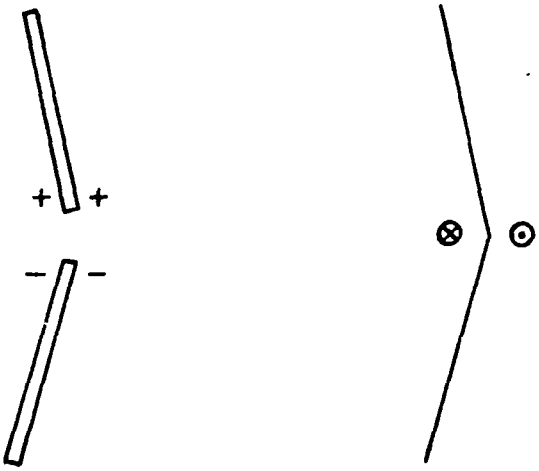

Fig. 13b. A two-sided slot is modeled with a magnetic doublet.

It is convenient to define a magnetic doublet as an array of two closely spaced parallel line sources with equal magnetic currents flowing in opposite directions. If the currents M_i are finite and the spacing tends to zero, the field $\underline{E}_i$ vanishes everywhere except in the narrow region between the two line sources. As indicated in Fig. 13b, the magnetic doublet provides a model for a "two-sided slot" in a conducting cylinder. This narrow axial slot radiates into the regions on both sides of the thin conducting wall. In this situation all the excitation voltages vanish except $V_g = M_i$, where mode g has the doublet at its terminals. This follows from superposition and Eqs. (34) and (37).

An axial slot with finite width is termed a "wide slot" to distinguish it from the previously considered "narrow slot" which has infinitesimal width. For simplicity assume a uniform electric field $E_a = V/a$ across the aperture, where V is the aperture voltage and "a" is the aperture width. Let the aperture width be divided into an integer number of equal segments with length h. The equivalent magnetic surface-current density over the aperture is $M_i = V/a$. For a two-sided wide slot, the excitation voltage vanishes for each mode outside the aperture region. From Eq. (11), the excitation voltages are

$$V_m = \frac{2(1 - \cos kh)\, V\, \epsilon_m}{ka \sin kh} \tag{38}$$

where ϵ_m is unity for the modes in the aperture and zero for those outside the aperture. At each edge of the aperture there will exist a mode having one segment in the aperture and another segment outside. For these two modes, ϵ_m is one-half.

For a one-sided wide slot the excitation voltages are just one-half those in Eq. (38), plus the contributions obtained by numerical integration (Eq. (11)) over the segments outside the aperture.

The complex power supplied by the aperture is

$$P = VI^* = \int_a \underline{J}_s^* \cdot \underline{E}_i \, d\ell \tag{39}$$

where V and I are the aperture voltage and current and the integration extends across the aperture. If the electric field is uniform across the aperture, $E_i = V/a$ for the two-sided case. It follows that the aperture current I is just the average value of J_s across the aperture. Thus

$$I = \sum_1^N \frac{V_m I_m}{V} \tag{40}$$

where V_m is given by Eq. (38).

For the one-sided aperture, $E_i = V/(2a)$ and the aperture current I is one-half the aperture-average of J_s. In all cases the aperture admittance is $Y = I/V$.

VIII. FAR-FIELD RADIATION AND SCATTERING

The scattered field of a cylinder is the sum of the free-space fields generated by the electric surface currents $\underline{J}_s$ and the magnetic surface currents $\underline{M}_s$ on the cylindrical surface. To obtain the total field we add the free-space field $(\underline{E}_i, \underline{H}_i)$ of the magnetic sources $\underline{M}_i$.

For a magnetic line source M_z of infinite length located on the z axis, the free-space field is

$$\underline{E} = \hat{\phi}\, jkM_z\, H_1(k\rho)/4 \tag{41}$$

$$\underline{H} = -\hat{z}\, k\, M_z\, H_0(k\rho)/(4\eta). \tag{42}$$

If the magnetic line source is parallel with the z axis and passes through the point (x,y), its free-space field at a distant point (ρ,ϕ) is

$$\underline{H} = -\frac{\hat{z}\, k\, M_z\, \sqrt{2j}\, e^{-jk\rho}\, e^{jk(x\cos\phi + y\sin\phi)}}{4\eta\, \sqrt{\pi k\rho}} \tag{43}$$

Consider a magnetic surface-current distribution $M_z(t)$ on a planar strip extending from (x_1,y_1) to (x_2,y_2) as in Fig. 14. Distance from the edge (x_1,y_1) to any point on the strip is measured by the coordinate t. For an arbitrary point on the strip,

$$x = x_1 + t\cos\alpha \tag{44}$$

$$y = y_1 + t\sin\alpha\,. \tag{45}$$

From Eq. (43), the free-space field of this source at a distant point (ρ,ϕ) is

$$\underline{H}^M = -\frac{\hat{z}\, k\, \sqrt{2j}\, e^{-jk\rho}\, e^{j\psi_1}}{4\eta\, \sqrt{\pi k\rho}} \int_0^h M_z(t)\, e^{jkct}\, dt \tag{46}$$

where

$$\psi_1 = k(x_1\cos\phi + y_1\sin\phi) \tag{47}$$

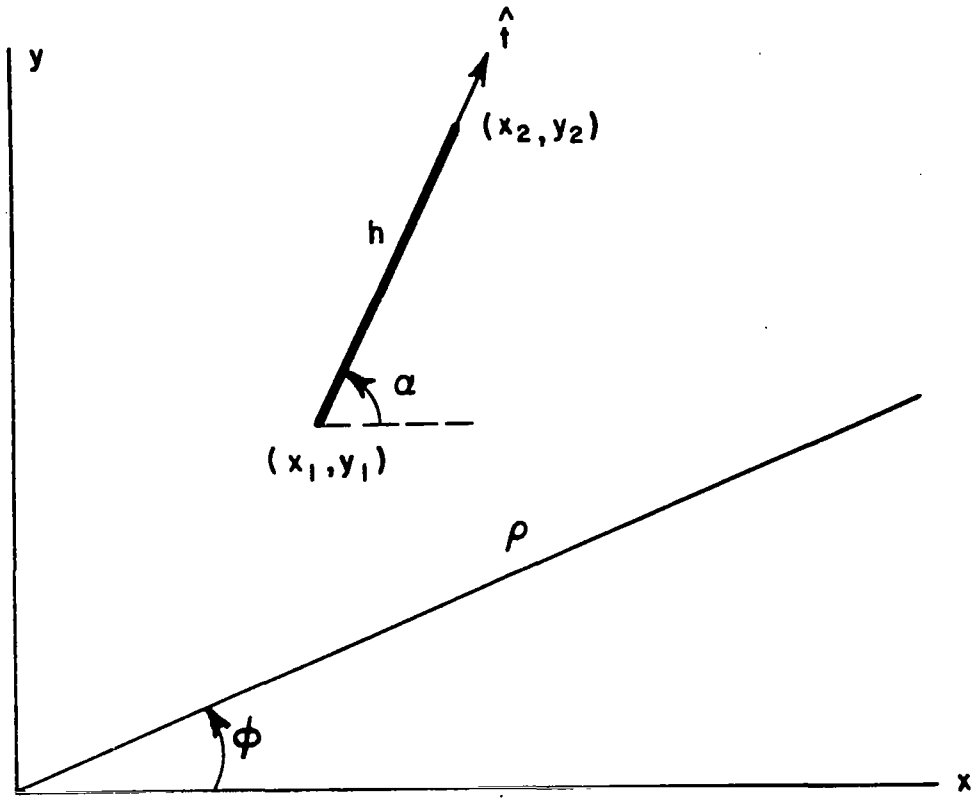

Fig. 14. A planar strip source extends from (x_1,y_1) to (x_2,y_2).

(48) $$\psi_2 = k(x_2 \cos\phi + y_2 \sin\phi)$$

(49) $$c = \cos(\alpha-\phi).$$

The free-space field of an electric surface current is given by Eq. (16). For an electric current $\underline{J} = \hat{t}\, J_t(t)$ on the strip in Fig. 14, the field at a distant point (ρ,ϕ) is

(50) $$\underline{H}^J = - \frac{\hat{z}\, k \sqrt{2j} \sin(\alpha-\phi)\, e^{-jk\rho}\, e^{j\psi_1}}{4\sqrt{\pi k\rho}} \int_0^h J_t(t)\, e^{jkct}\, dt.$$

It may be noted that Eq. (50) is similar to Eq. (46).

If the magnetic surface-current density $M_z(t)$ in Eq. (46) arises through the finite conductivity of the cylinder, the impedance boundary condition in Eq. (6) yields

$$M_z(t) = s\, Z_s\, J_t(t) \tag{51}$$

where

$$s = (\hat{t} \times \hat{n})\cdot\hat{z} = \pm 1 \tag{52}$$

and the unit normal $\hat{n}$ is directed into the source region.

From Eqs. (46), (50) and (51) the distant scattered field from one segment of the conducting cylinder (the strip in Fig. 14) is

$$H_z^s = - \frac{\sqrt{2j}\ (\eta \sin(\alpha-\phi) + s\, Z_s)\ e^{-jk\rho}\ F}{4\eta\ \sqrt{\pi k\rho}\ \sin kh} \tag{53}$$

where

$$F = k \sin(kh)\ e^{j\psi_1} \int_0^h J_t(t)\ e^{jkct}\ dt. \tag{54}$$

If the electric current on this segment has a sinusoidal distribution as follows:

$$J_t(t) = \frac{I_1 \sin(kh-kt) + I_2 \sin(kt)}{\sin(kh)} \tag{55}$$

Eq. (54) yields

$$F = \frac{I_1}{\sin^2(\alpha-\phi)}\ [e^{j\psi_2} - (\cos kh + j\, c \sin kh)\ e^{j\psi_1}] + \frac{I_2}{\sin^2(\alpha-\phi)}\ [e^{j\psi_1} - (\cos kh - j\, c \sin kh)\ e^{j\psi_2}]. \tag{56}$$

In the end-fire directions where $(\alpha-\phi)$ is zero or pi, Eq. (54) yields

$$F = [e^{j\psi_1} \sin kh - kh\, e^{j\psi_2}]\, jcI_1/2 - [e^{j\psi_2} \sin kh - kh\, e^{j\psi_1}]\, jcI_2/2. \tag{57}$$

The field scattered by the cylinder is obtained by summing the contributions from all the segments of the cylinder.

In plane-wave scattering problems, one is usually interested in the echo width W defined as follows:

$$W = \lim_{\rho \to \infty} 2\pi\rho \, |H^s/H^i|^2 \tag{58}$$

where H^i is the incident magnetic field intensity.

In antenna and radiation problems we are interested in the directive gain:

$$G = P(\phi)/P_{av} \tag{59}$$

where $P(\phi)$ is the power density in direction ϕ and P_{av} is the average power density:

$$P_{av} = \frac{1}{2\pi} \int_0^{2\pi} P(\phi)\, d\phi. \tag{60}$$

The power radiated per unit length of cylinder is

$$W_r = 2\pi\rho \, P_{av}. \tag{61}$$

For a perfectly conducting cylinder, an alternative expression is

$$W_r = |V|^2 \, G \tag{62}$$

where V is the terminal voltage and G is the conductance per unit length. From Eqs. (59) and (61),

$$G = \frac{2\pi\rho\eta \, |H_z|^2}{W_r} \tag{63}$$

IX. NUMERICAL RESULTS

Figure 15 presents the backscattering echo width of circular

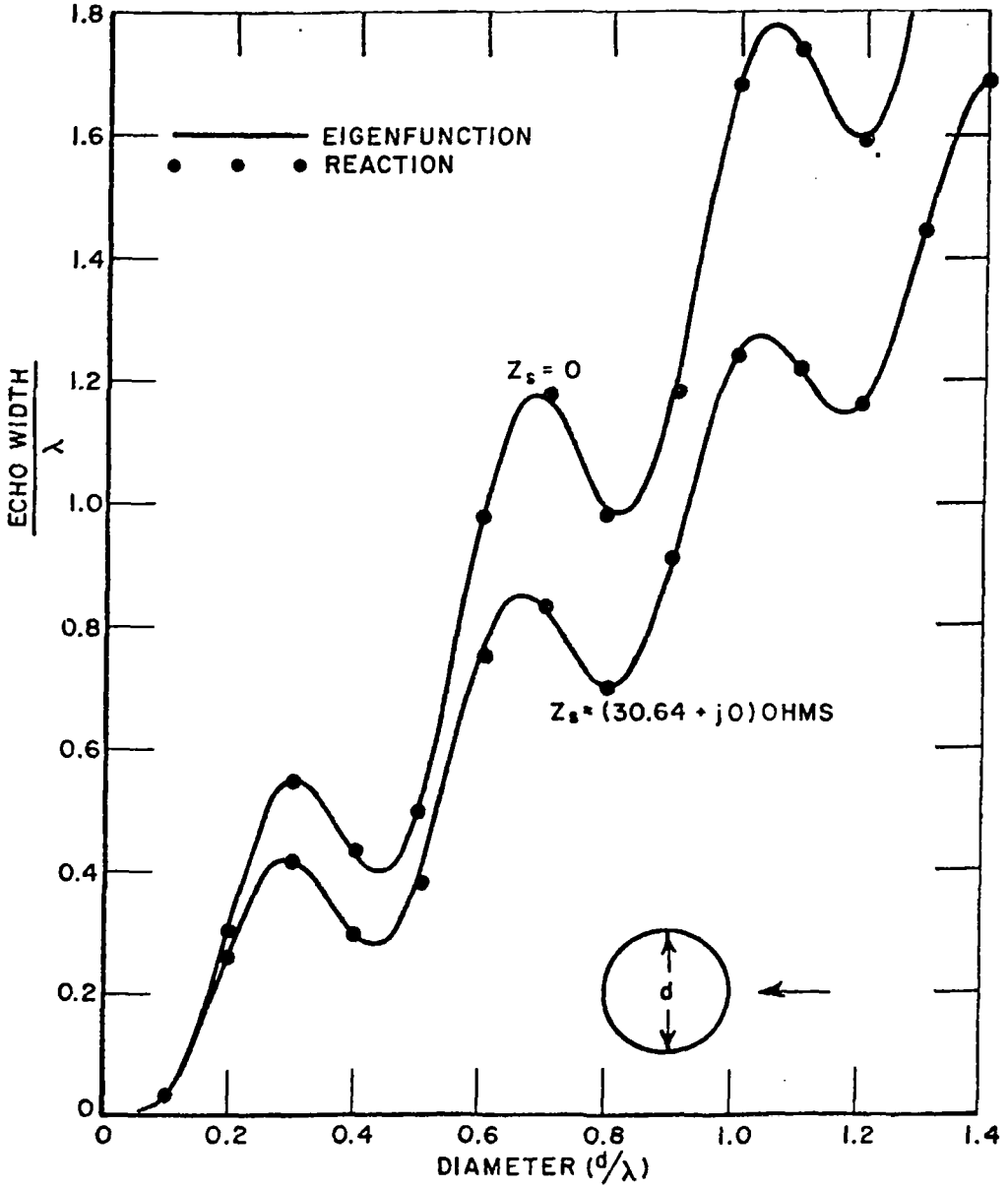

Fig. 15. Backscattering echo width of circular cylinder for TE polarization.

cylinders with perfect and imperfect conductivity. In the reaction calculations the cylinder was divided into N segments where N = 12 + 20 d/λ and d is the diameter. Figure 16 shows similar results for a

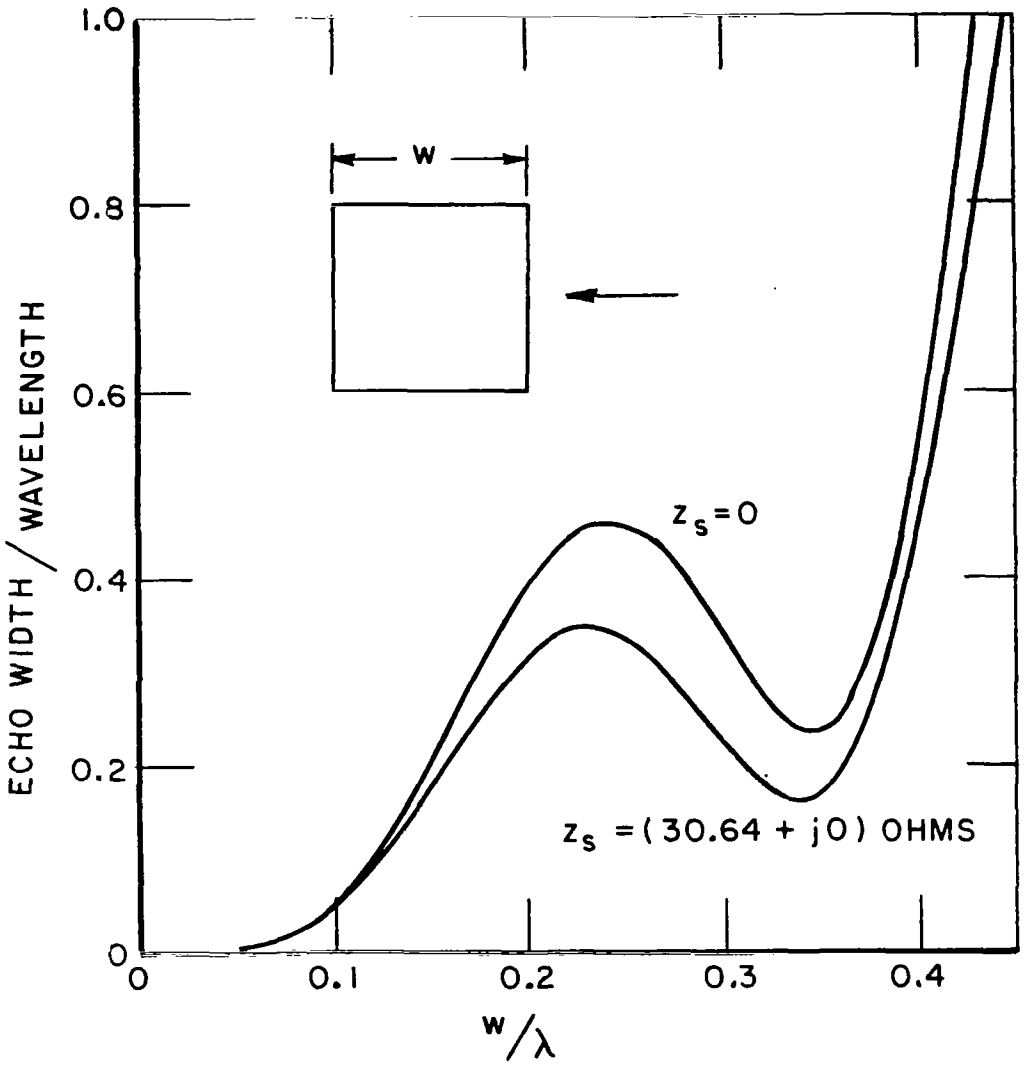

Fig. 16. Broadside backscatter of square cylinder for TE polarization.

square cylinder with 16 segments. Figure 17 illustrates the back-scattering characteristics of a circular-sector cylinder. Our data in Fig. 17 show excellent agreement with independent calculations by Billingsley and Sinclair[15]. The echo width of the complete circular cylinder is 2.224 λ.

Figure 18 shows the conductance of a narrow axial slot in a circular cylinder. The number of segments is $N = 16 + 20\ d/\lambda$ for

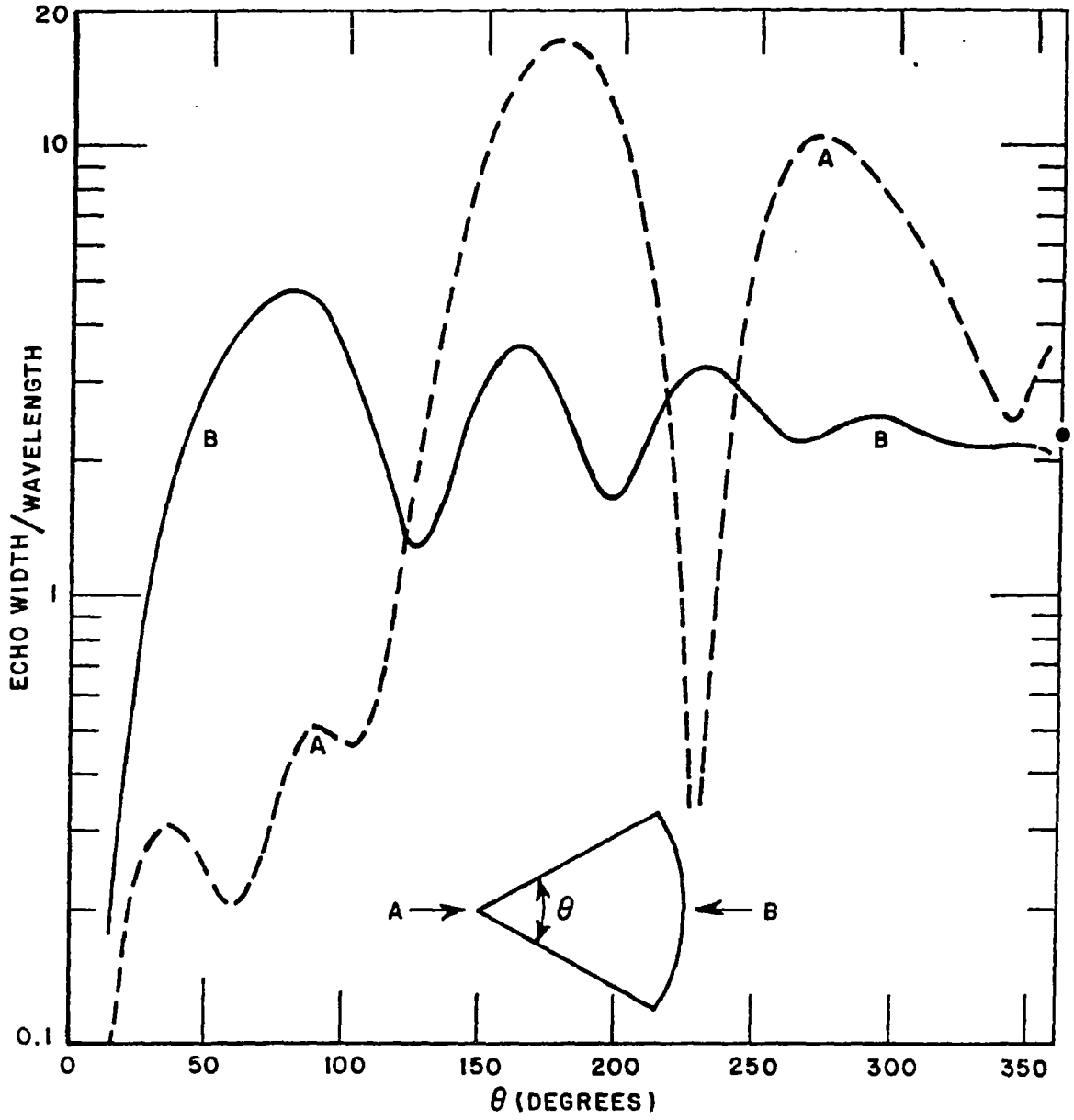

Fig. 17. Backscatter echo width of perfectly conducting circular-sector cylinder for TE polarization. (Radius: ka = 5)

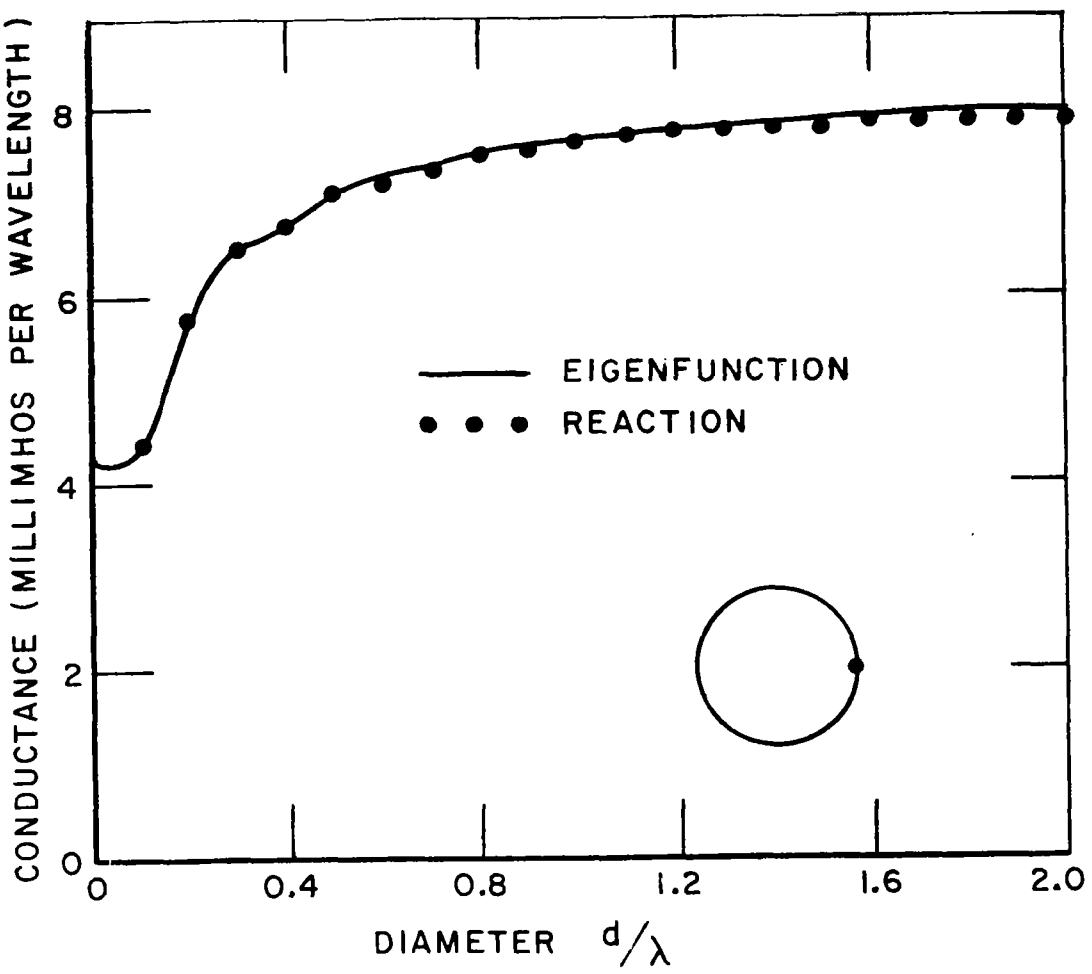

Fig. 18. Conductance of narrow axial slot in perfectly conducting circular cylinder for TE polarization.

diameters up to one wavelength and N = 56 for the larger cylinders. Figure 19 shows similar results for a square cylinder with N = 24 + 20 w/λ where w is the width of the cylinder.

Two methods are available for determining the conductance of a narrow axial slot. The simpler and faster method is to take the real part of the electric surface-current density at the slot, and the alternative is to integrate the far-field power pattern. The two methods generally show good agreement if the cylinder is divided into an adequate number of segments. For closed noncircular cylinders, however, the first method fails when interior modes resonate. With a square cylinder, this occurs when the width w is a multiple of λ/2. No difficulty is encountered in calculating the echo width or the gain of a source on or near the cylinder. The conductance data in Fig. 19 were obtained by far-field integration.

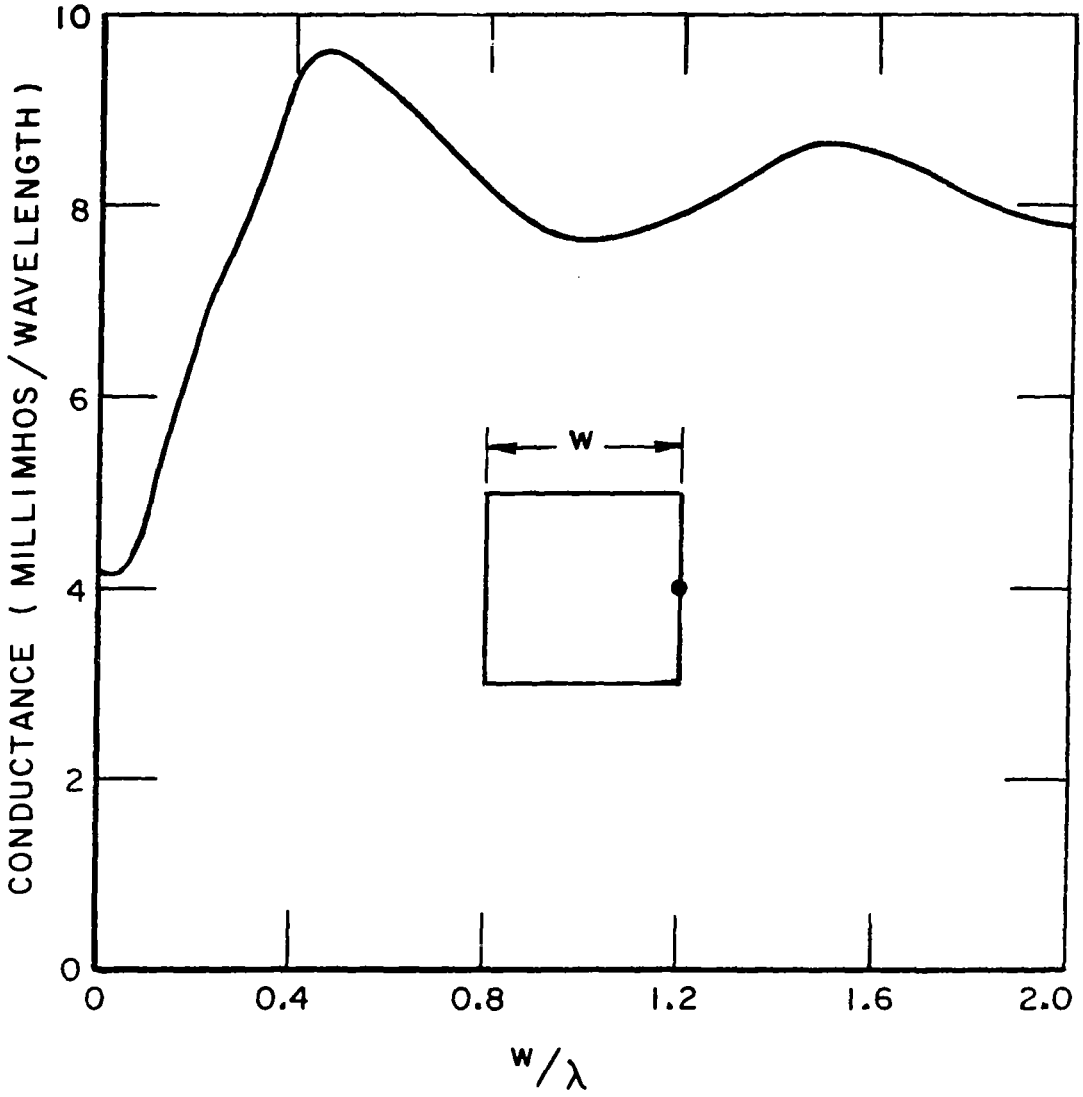

Fig. 19. Conductance of narrow axial slot on perfectly conducting square cylinder.

Figure 20 shows the forward gain and backward gain of a narrow axial slot in a circular cylinder.

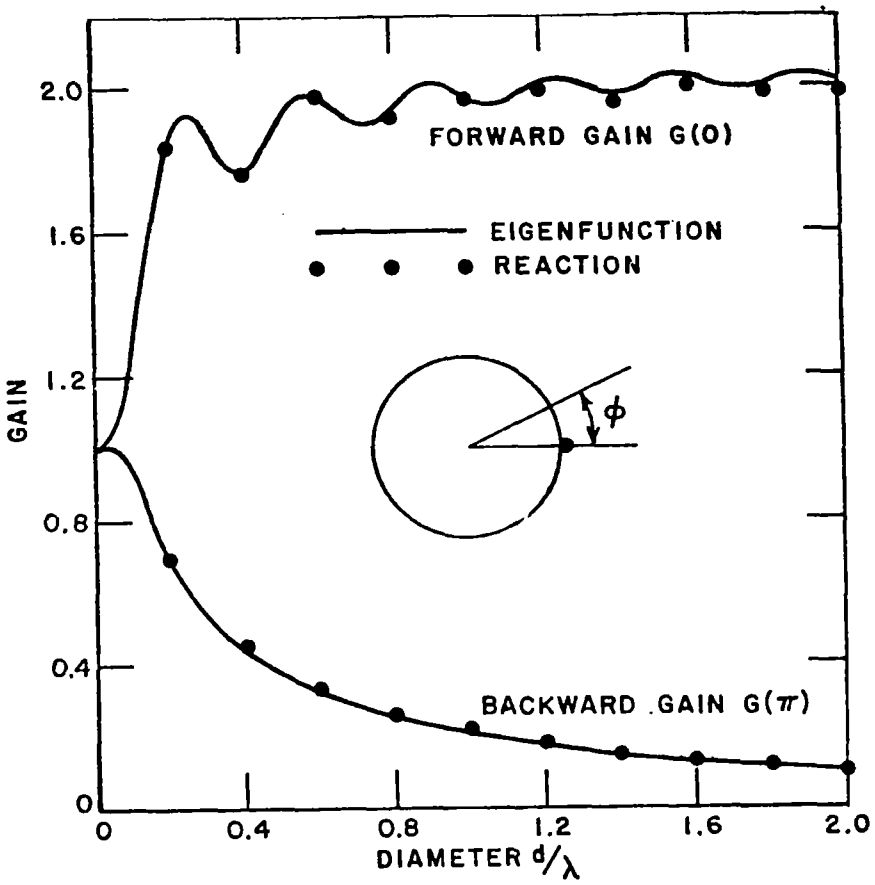

Fig. 20. Directive gain of narrow axial slot on perfectly conducting circular cylinder for TE polarization.

Figure 21 illustrates the conductance of a wide axial slot in a circular cylinder with 56 segments, and Fig. 22 shows similar data for a square cylinder. These conductance data apply when the tangential electric field has a uniform distribution across the aperture.

Figures 23 and 24 show the gain patterns of a magnetic line source near a circular and square cylinder, respectively.

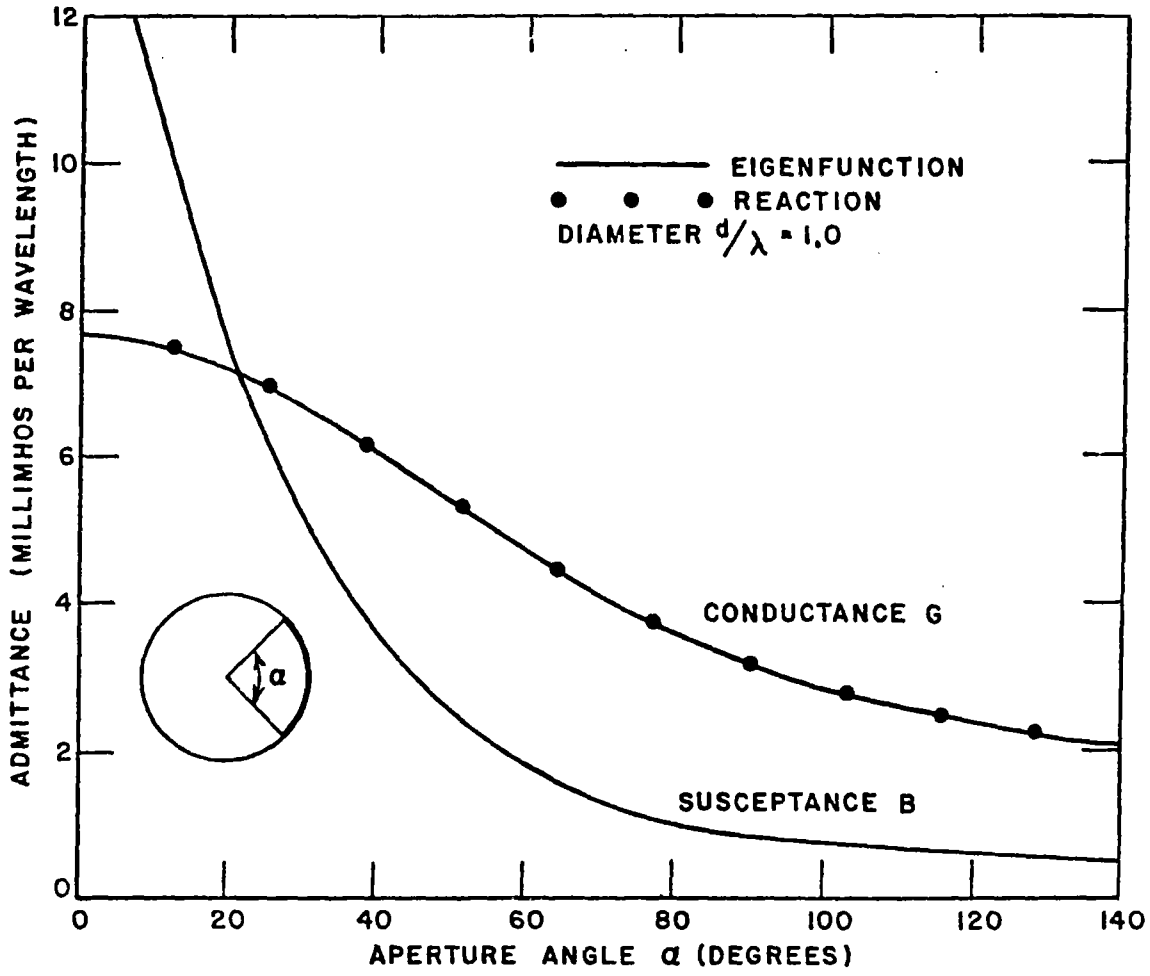

Fig. 21. Admittance of wide axial slot in perfectly conducting circular cylinder for TE polarization.

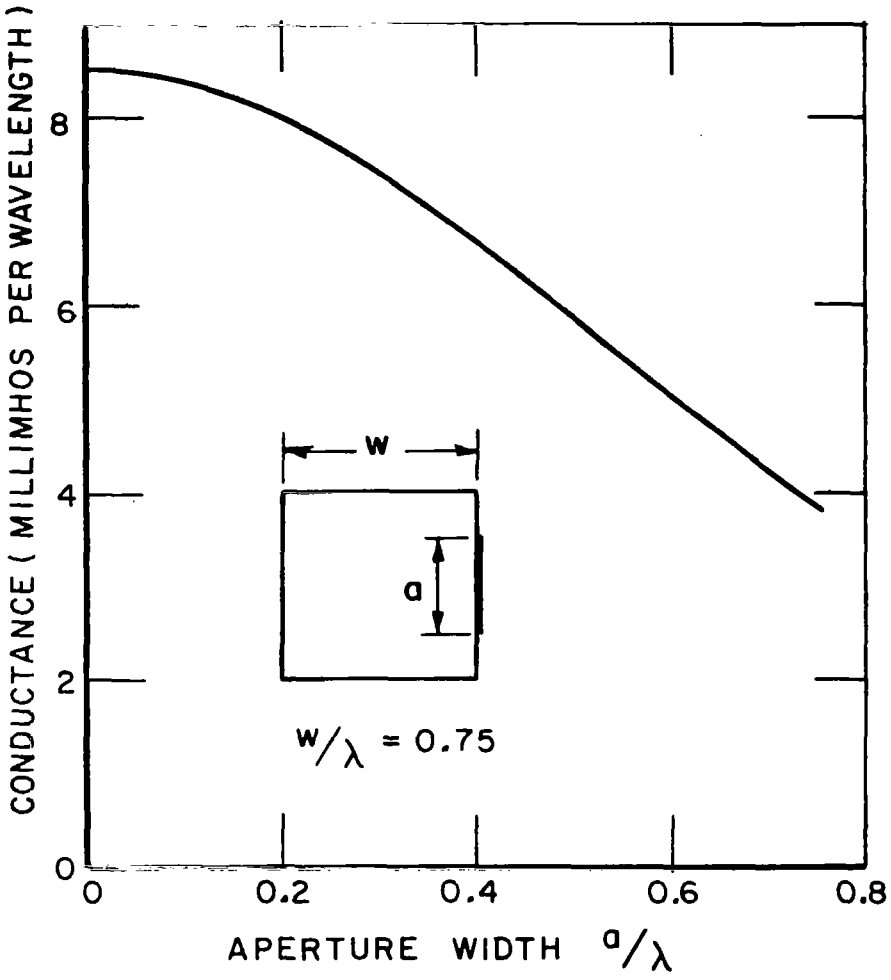

Fig. 22. Conductance of wide axial slot in perfectly conducting square cylinder for TE polarization.

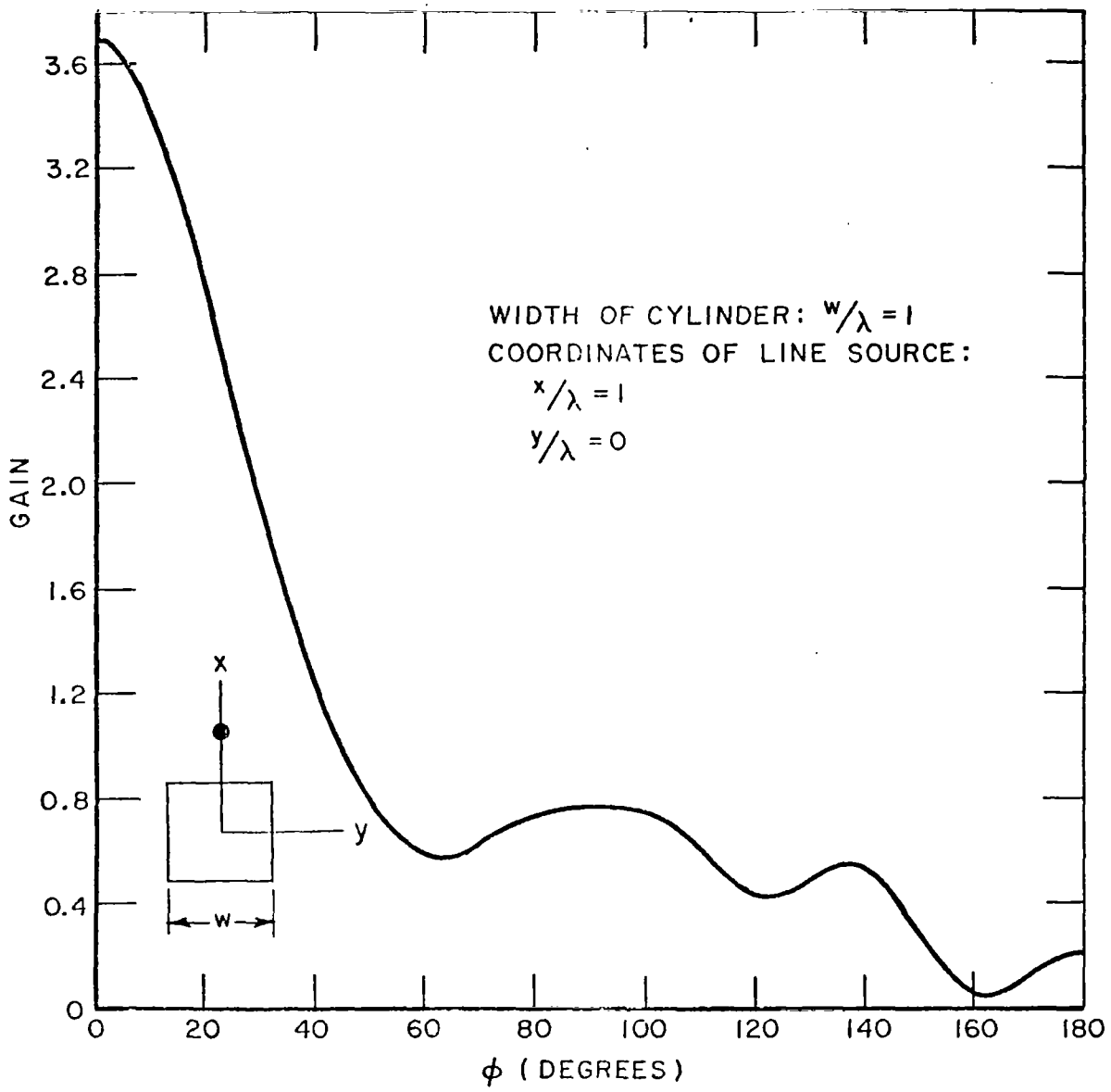

Fig. 24. Gain $G(\phi)$ of magnetic line source near a perfectly conducting square cylinder.

For perfectly conducting strips, our calculations show excellent agreement with the eigenfunction solution for broadside backscatter and the far-field patterns of one-sided and two-sided narrow axial slots. We also have excellent agreement with the eigenfunction solution for the far-field pattern of a narrow axial slot in an elliptic cylinder[16]. For a magnetic line source near a square cylinder and an open circular-arc cylinder, we have excellent agreement with the geometrical theory of diffraction.

X. SUMMARY

This report presents the piecewise-sinusoidal reaction formulation for TE radiation and scattering from noncircular conducting cylinders. Numerical results are included to show the backscattering echo width of circular and square cylinders with perfect and imperfect conductivity. Additional data illustrate the admittance and gain of axial-slot antennas on circular and square cylinders and the gain of a magnetic line source near a cylinder. The computer program and subroutines are presented in Appendices.

REFERENCES

1. Mei, K.K. and Van Bladel, J.G., "Scattering by Perfectly-Conducting Rectangular Cylinders," IEEE Trans., Vol. AP-11, March 1963, pp. 185-192.

2. Andreasen, M.G., "Scattering from Parallel Metallic Cylinders With Arbitrary Cross Sections," IEEE Trans., Vol. AP-12, November 1964, pp. 746-754.

3. Mullin, C.R., Sandburg, R. and Velline, C.O., "A Numerical Technique for the Determination of Scattering Cross Sections of Infinite Cylinders of Arbitrary Geometrical Cross Section," IEEE Trans., Vol. AP-13, January 1965, pp. 141-149.

4. Richmond, J.H., "Scattering by an Arbitrary Array of Parallel Wires," IEEE Trans., Vol. MTT-13, July 1965, pp. 408-412.

5. Wallenberg, R.F. and Harrington, R.F., "Radiation From Apertures in Conducting Cylinders of Arbitrary Cross Section," IEEE Trans., Vol. AP-17, January 1969, pp. 56-62.

6. Shafai, L., "An Improved Integral Equation for the Numerical Solution of Two-Dimensional Diffraction Problems," Canadian Journal of Physics, Vol. 48, 1970, pp. 954-963.

7. Bennett, C.L. and Weeks, W.L., "Transient Scattering from Conducting Cylinders," IEEE Trans., Vol. AP-18, September 1970, pp. 627-633.

8. Wilton, D.R. and Mittra, Raj, "A New Numerical Approach to the Calculation of Electromagnetic Scattering Properties of Two-Dimensional Bodies of Arbitrary Cross Section," IEEE Trans., Vol. AP-20, May 1972, pp. 310-317.

9. Rumsey, V.H., "Reaction Concept in Electromagnetic Theory," Physical Review, Vol. 94, June 15, 1954, pp. 1483-1491.

10. Jones, D.S., "A Critique of the Variational Method in Scattering Problems," IEEE Trans., Vol. AP-4, July 1956, pp. 297-301.

11. Cohen, M.H., "Application of the Reaction Concept to Scattering Problems," IEEE Trans., Vol. AP-3, October 1955, pp. 193-199.

12. Harrington, R.F., Time-Harmonic Electromagnetic Fields, McGraw-Hill, New York, 1961, pp. 340-345.

13. Richmond, J.H., "A Reaction Theorem and its Application to Antenna Impedance Calculations," IEEE Trans., Vol. AP-9, November 1961, pp. 515-520.

14. Schelkunoff, S.A., "On Diffraction and Radiation of Electromagnetic Waves," Physical Review, Vol. 56, August 15, 1939.

15. Billingsley, J.B. and Sinclair, G., "Numerical Solutions to Electromagnetic Scattering from Strips, Finite Wedges, and Notched Circular Cylinders," Canadian Journal of Physics, Vol. 44, 1966, pp. 3217-3225.

16. Sinclair, George, "The Patterns of Antennas Located Near Cylinders of Elliptical Cross Section," I.R.E. Proceedings, Vol. 39, No. 6, June 1951, pp. 660-668.

17. Handbook of Mathematical Functions, U.S. Department of Commerce, National Bureau of Standards, Applied Mathematics Series AMS-55, pp. 369-370.

18. Hildebrand, F.B., Methods of Applied Mathematics, Prentice-Hall, New York, 1952.

APPENDIX I
MAIN COMPUTER PROGRAM

The main computer program is listed in Fig. 25 in the Fortran language. With finite conductivity, the program handles a closed cylinder or an array of closed cylinders. With perfect conductivity, the program handles open cylinders, closed cylinders, more complicated cylinders as in Fig. 10, and arrays of cylinders. By setting the integer LOP, the user may select any one of the four excitation options listed below.

1. If LOP = 1, transfer to statement 110 for two-sided narrow axial slot.

2. If LOP = 2, transfer to statement 120 for two-sided wide axial slot.

3. If LOP = 3, transfer to statement 130 for magnetic line source or one-sided narrow axial slot.

4. If LOP = 4, transfer to statement 140 for plane-wave scattering.

Statement 10 reads the first input data defined as follows:

IWR Positive or negative integer to write or suppress the current distribution

LOP Integer to select option 1, 2, 3 or 4

NM Number of segments (monopoles) on the contour of the cylinder

NP Number of points on the contour.

Figures 26 and 27 illustrate typical input data for a square cylinder and a strip, respectively. The square cylinder has four segments and four points, and the strip has four segments and 5 points. (In practice we would divide the contour into a larger number of segments for more accurate results.) For a closed cylinder with finite conductivity, the points must be numbered in the counterclockwise direction (as in Fig. 26) for exterior excitation, and in the clockwise direction for interior excitation. For perfectly conducting cylinders, the points and segments may be numbered randomly.

Next we must give the computer information to indicate which points are joined with conducting segments. This data is read in the DO LOOP ending with statement 50. IA(J) and IB(J) are the index numbers of the endpoints of segment J. The segments must be numbered consecutively from 1 through NM. The DO LOOP ending with statement 60 reads the coordinates XC(I) and YC(I) of the points in arbitrary units. These points, which lie on the contour of the cylinder and define its shape and size, must be numbered consecutively from 1 through NP. From XC(I) and YC(I), the computer will determine X(I) and Y(I) which denote $2\pi x/\lambda$ and $2\pi y/\lambda$. Statement 80 reads the following data:

CMM — Conductivity in megamhos per meter. A negative value indicates perfect conductivity.

DPH — Increment in the far-field angle ϕ in degrees.

FMC — Frequency in megahertz.

SCALE — Scale factor for multiplying XC and YC to obtain the coordinates in meters. A negative value indicates the unit of measure for XC and YC is the wavelength.

TC — Thickness of conductor in same units as XC and YC. TC is not needed if the cylinder has perfect conductivity.

For option 1 (two-sided narrow axial slot), statement 110 reads the index number IGN of the mode which has the generator at its terminals. The modes are set up in subroutine SORT, and statement 55 writes a list of these modes. Mode I has terminals at the point I2(I) and endpoints at I1(I) and I3(I). The reference direction for the modal current is from I1 toward I3, and the reference polarity for the modal voltage is negative at I1 and positive at I3.

Table V shows the list of modes for the square cylinder and the

TABLE V

OUTPUT DATA

Mode definitions for square cylinder in Fig. 26

I	I1(I)	I2(I)	I3(I)
1	4	1	2
2	1	2	3
3	2	3	4
4	3	4	1

Y11 = .00459 + j .00341
Gain = 1.166 at ϕ = 0
Gain = 0.835 at ϕ = 180°

Mode definitions for strip in Fig. 27

I	I1(I)	I2(I)	I3(I)
1	1	2	3
2	2	3	4
3	3	4	5

Scattering cross-section = 0.00163
Backscatter echo width = 0.00328

strip. Four modes are defined on the square cylinder, and the terminals of mode I are located at point I. Thus to indicate a two-sided narrow axial slot at the lower-right corner of the square, we set IGN = 1. Three modes are defined on the strip, and the terminals of mode I are located at point I + 1. To indicate a slot at the center of the strip we set IGN = 2.

For more complicated cylinders (such as in Fig. 10), it is necessary to make a preliminary computer run to obtain the mode definitions. Then we can select IGN from the mode list and proceed with the final computer run. It is important to note that IGN is a mode number and is not always the same as the index number of the point where the slot is located. With option 1, the computer will write out the slot admittance Y11 and proceed to calculate the power gain GAIN with increments DPH in the far-field angle PH.

With option 2 (two-sided wide axial slot), statement 120 reads the index numbers JSA and JSB of the first and last segments in the aperture. It is assumed that JSB is greater than or equal to JSA and that the segments are numbered consecutively across the aperture. The computer writes out the admittance Y11 and the gain of the wide slot.

For option 3 (magnetic line source or one-sided narrow axial slot), statement 130 reads the angle PSI in degrees and the coordinates XCS and YCS of the line source in the same units employed for XC and YC. PSI is defined in Fig. 12 and Eq. (34) and is used only when the line source is located at one of the points (XC,YC) on the contour of the cylinder. The computer writes out the admittance Y11 and the gain. For a unit magnetic line source, the admittance is defined as the magnetic field H_z at the line source. The singular term in the susceptance is suppressed, and the scattered field H_z^s is calculated by integrating over the currents $\underline{J}_s$ and $\underline{M}_s$ on the cylinder.

With option 4 (plane-wave scattering), statement 140 reads BSC and PHI. Set BSC positive or negative for backscattering or bistatic data, respectively. For bistatic scattering, PHI is the angle of incidence in degrees. The computer writes the scattering angle PH in degrees, the echo width EWL in wavelengths, and (in a backscattering situation) the extinction cross-section ECS in wavelengths.

The radiated or scattered power is calculated by numerical integration of the far-field power pattern. This result is employed to calculate the radiation conductance GR or the scattering cross-section SCS immediately below statement 280. These quantities will not be accurate, however, unless the angular increment DPH is sufficiently small. For a perfectly conducting cylinder, ECS should be equal to SCS and GR should be equal to the real part of Y11.

In some radiation problems the admittance Y11 will be inaccurate and, as a result, the power gain GAIN will have incorrect normalization. This occurs with an axial slot on a closed noncircular cylinder in the vicinity of an interior resonance. Even in this case, GAIN is useful as the relative far-field power pattern. (The pattern is correct even when the normalization is not.) For perfectly conducting cylinders, this situation is indicated when GR differs appreciably from the real part of Y11.

Finally, the computer reads JOB and LOP below statement 280. If JOB = 10, transfer is made to statement 10 to undertake a new problem. If JOB = 80, transfer goes to statement 80 for further calculations on a previously considered cylinder with a new conductivity, frequency, scale or thickness. If JOB = 300, transfer goes to statement 300 to terminate the calculations. If JOB does not equal one of these three numbers, transfer goes to statement 110, 120, 130 or 140 according to LOP. This is appropriate when we wish to change only the excitation of the cylinder.

In the DATA statement near the beginning of the program, IDM denotes the dimensions of the subscripted quantities and INT controls the accuracy of certain integrations performed in the subroutines. Although INT = 10 is suitable, one may use a smaller or larger value to increase the computational speed or the accuracy, respectively.

```
      COMPLEX COT,ZS,Z11,Z12,Y11,Y12,HZM-HZS,HZT
      COMPLEX C(56,56),CJ(56),HJJ(56),HMM(56),VJ(56)
      DIMENSION IA(56),IB(56),I1(56),I2(56),I3(56),JA(56),JB(56)
      DIMENSION MD(56,5),ND(56),X(56),Y(56),D(56),XC(56),YC(56),DC(56)
      DATA IDM,INT/56,10/
      DATA PI,TP,ETA/3.14159,6.28318,376.727/
    2 FORMAT(1X,8F15.7)
    5 FORMAT(1H0)
    7 FORMAT(7F10.5)
    8 FORMAT(1X,14I5)
      COT=1.414214*ETA*CMPLX(1.,-1.)
   10 READ(5,8)IWR,LOP,NM,NP
      WRITE(6,8)IWR,LOP,NM,NP
      WRITE(6,5)
      DO 50 J=1,NM
      READ(5,8)IA(J),IB(J)
   50 WRITE(6,8)J,IA(J),IB(J)
      WRITE(6,5)
      CALL SORT(IA,IB,I1,I2,I3,JA,JB,MD,ND,NM,NP,N,IDM,MAX,MIN)
      IF(MIN.LT.1 .OR. MAX.GT.5)GO TO 300
      DO 55 I=1,N
   55 WRITE(6,8)I,I1(I),I2(I),I3(I)
      WRITE(6,5)
      DO 60 I=1,NP
      READ(5,7)XC(I),YC(I)
      FI=I
   60 WRITE(6,2)FI,XC(I),YC(I)
      WRITE(6,5)
      DO 70 JAN=1,NM
      KIM=IA(JAN)
      LIM=IB(JAN)
   70 DC(JAN)=SQRT((XC(LIM)-XC(KIM))**2+(YC(LIM)-YC(KIM))**2)
   80 READ(5,7)CMM,DPH,FMC,SCALE,TC
      WRITE(6,2)CMM,DPH,FMC,SCALE,TC
      WRITE(6,5)
      WAVM=300./FMC
      TPL=TP
      IF(SCALE.GT.0.)TPL=TP*SCALE/WAVM
      DO 90 IAN=1,NP
      X(IAN)=TPL*XC(IAN)
   90 Y(IAN)=TPL*YC(IAN)
      DO 95 JAN=1,NM
   95 D(JAN)=TPL*DC(JAN)
      I12=1
      ISYM=0
      ZS=(.0,.0)
      TK=TPL*TC
      IF(CMM.GT.0.)CALL CSURF(CMM,FMC,TK,ZS)
      IF(CMM.GT.0.)ISYM=1
      CALL CDANT(C,D,X,Y,ZS,IA,IB,I1,I2,I3,ISYM
     B,IDM,INT,JA,JB,MD,N,ND,NM,NP)
      IF(ISYM.EQ.10)GO TO 300
      GO TO (110,120,130,140),LOP
  110 READ(5,8)IGN
      CALL VNAS(IDM,IGN,ISYM,IWR,I12,D,C,CJ,Y11)
      FGN=IGN
      WRITE(6,2)FGN,Y11
      GO TO 200
  120 READ(5,8)JSA,JSB
      CALL VWAS(IA,IB,IDM,ISYM,IWR,I1,I2,I3,I12,JSA,JSB,MD,N,ND,NM
     2,C,CJ,D,VJ,Y11)
      FSA=JSA
```

Fig. 25. The MAIN computer program.

```
      FSB=JSB
      WRITE(6,2)FSA,FSB,Y11
      GO TO 200
  130 READ(5,7)PSI,XCS,YCS
      XS=TPL*XCS
      YS=TPL*YCS
      CALL VMLS(IA,IB,IDM,INT,ISYM,IWR,I1,I2,I3,I12,MD,N,ND,NM,
     2C,CJ,D,PSI,VJ,X,Y,XS,YS,Y11,ZS)
      WRITE(6,2)PSI,XCS,YCS,Y11
      GO TO 200
  140 READ(5,7)BSC,PHI
      WRITE(6,2)BSC,PHI
  200 WRITE(6,5)
      IF(LOP.NE.4)G=REAL(Y11)
      INC=-1
      IF(LOP.EQ.4)INC=1
      IPA=2
      IF(LOP.EQ.4)IPA=1
      IF(LOP.NE.4)BSC=-1.
      NPH=360./DPH+1.5
      GR=.0
      DO 280 IPH=IPA,NPH
      FPH=IPH-2
      PH=DPH*FPH
      IF(IPH.EQ.1)PH=PHI
      CALL VFF(IA,IB,INC,IDM,ISYM,IWR,I1,I2,I3,I12,LOP,MD,N,ND,NM,
     2C,CJ,D,EWL,G,GAIN,HJJ,HMM,HZS,HZT,PH,ECS,VJ,X,Y,XS,YS,ZS)
      IF(LOP.NE.4)WRITE(6,2)PH,GAIN
      IF(LOP.EQ.4)WRITE(6,2)PH,EWL,ECS
      INC=-1
      IF(BSC.GT.0.)INC=1
  280 GR=GR+CABS(HZT)**2
      WRITE(6,5)
      SCS=.0174533*DPH*GR
      IF(LOP.EQ.4)WRITE(6,2)SCS
      GR=ETA*SCS
      IF(LOP.NE.4)WRITE(6,2)GR
      WRITE(6,5)
      READ(5,8)JOB,LOP
      IF(JOB.EQ.10)GO TO 10
      IF(JOB.EQ.80)GO TO 80
      IF(JOB.EQ.300)GO TO 300
      GO TO(110,120,130,140),LOP
  300 CONTINUE
      CALL EXIT
      END
```

Fig. 25. (Continued)

Card Number							
1	-1	3	4	4			
2	1	2					
3	2	3					
4	3	4					
5	4	1					
6		.5		-.5			
7		.5		.5			
8		-.5		.5			
9		-.5		-.5			
10		-1.		180.	300.	.1	.001
11		90.		.5	-.5		
12	300	1					

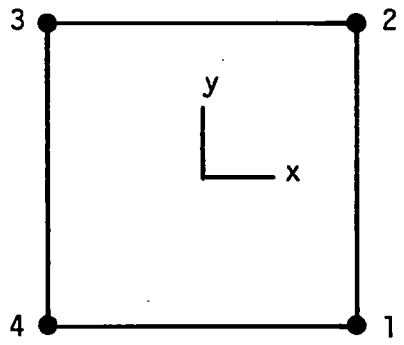

Fig. 26. Input data for square cylinder with one-sided narrow axial slot. The diagram shows the numbering system for the four points on the cylinder.

Card Number							
1	-1	4	4	5			
2	1	2					
3	2	3					
4	3	4					
5	4	5					
6		-.5		.0			
7		-.25		.0			
8		.0		.0			
9		.25		.0			
10		.5		.0			
11		-1.		90.	300.	.1	.001
12		-1.		90.			
13	300	1					

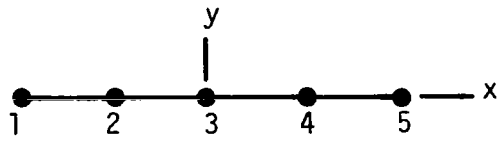

Fig. 27. Input data for bistatic scattering by strip. The diagram shows the numbering system for the five points on the strip.

APPENDIX II
Subroutine SORT

Subroutine SORT, listed in Fig. 28, defines a set of strip-dipole mode currents on the cylinder. The input data IA, IB, NM, NP and IDM have been defined already. The output data are defined as follows:

N	Number of dipole modes on the cylinder
I1(I)	Endpoint on dipole I
I2(I)	Terminal point on dipole I
I3(I)	Endpoint on dipole I
JA(I)	Segment of dipole I
JB(I)	Segment of dipole I
ND(J)	Number of dipoles sharing segment J
MD(J,K)	A list of the dipoles sharing segment J
MAX, MIN	Extreme values of ND(J).

At completion of the DO LOOP ending with statement 20, NJK denotes the number of segments intersecting at point K, and JSP is a list of these segments. In the DO LOOP ending with statement 22, the computer sets up the appropriate number MOD of dipole modes with terminals at point K. The first mode is set up on segments JSP(1) and JSP(2), the second mode on JSP(1) and JSP(3), etc. Since the segments are listed in ascending order in JSP, all the modes with terminals at point K will share the lowest-numbered segment JSP(1) having an endpoint at K.

LAX denotes the largest number of segments intersecting at any point, and LIN denotes the smallest.

```
      SUBROUTINE SORT(IA,IB,I1,I2,I3,JA,JB,MD,ND,NM,NP,N,IDM,MAX,MIN)
      DIMENSION JSP(10),MD(IDM,5),ND(IDM)
      DIMENSION IA(IDM),IB(IDM),I1(IDM),I2(IDM),I3(IDM),JA(IDM),JB(IDM)
      I=0
      LAX=0
      LIN=100
      DO 24 K=1,NP
      NJK=0
      DO 20 J=1,NM
      IND=(IA(J)-K)*(IB(J)-K)
      IF(IND.NE.0)GO TO 20
      NJK=NJK+1
      JSP(NJK)=J
   20 CONTINUE
      IF(NJK.GT.LAX)LAX=NJK
      IF(NJK.LT.LIN)LIN=NJK
      MOD=NJK-1
      IF(MOD.LE.0)GO TO 24
```

Fig. 28. Subroutine SORT.

```
      JAI=JSP(1)
      III=IA(JAI)
      IF(IA(JAI).EQ.K)III=IB(JAI)
      DO 22 IMD=1,MOD
      I=I+1
      NJK=IMD+1
      JA(I)=JAI
      JBI=JSP(NJK)
      JB(I)=JBI
      I1(I)=III
      I2(I)=K
      I3(I)=IA(JBI)
      IF(IA(JBI).EQ.K)I3(I)=IB(JBI)
   22 CONTINUE
   24 CONTINUE
      IF(LAX.NE.2 .OR. LIN.NE.2)GO TO 26
      III=I1(1)
      I1(1)=I3(1)
      I3(1)=III
      JA1=JA(1)
      JA(1)=JB(1)
      JB(1)=JA1
   26 N=I
      DO 30 J=1,NM
      ND(J)=0
      DO 30 K=1,5
   30 MD(J,K)=0
      DO 40 I=1,N
      J=JA(I)
      DO 38 L=1,2
      ND(J)=ND(J)+1
      K=1
      M=0
   32 MJK=MD(J,K)
      IF(MJK.NE.0)GO TO 34
      M=1
      MD(J,K)=I
   34 K=K+1
      IF(K.GT.5)GO TO 38
      IF(M.EQ.0)GO TO 32
   38 J=JB(I)
   40 CONTINUE
      MIN=100
      MAX=0
      DO 46 J=1,NM
      NDJ=ND(J)
      IF(NDJ.GT.MAX)MAX=NDJ
   46 IF(NDJ.LT.MIN)MIN=NDJ
      RETURN
      END
```

Fig. 28. (Continued)

APPENDIX III
Subroutine CDANT

Subroutine CDANT, listed in Fig. 29, sets up the impedance matrix Z_{ij} defined by Eqs. (9) and (10) and denoted in the computer program by C(I,J). Most of the input data have been defined already; the new items are defined as follows:

D(J)	kd_j where d_j is the length of segment j and $k = 2\pi/\lambda$
X(I),Y(I)	kx_i and ky_i where (x_i, y_i) are the coordinates of point i
ZS	surface impedance in ohms
ISYM	zero or one for perfectly conducting or finitely conducting cylinder, respectively.

The surface impedance ZS is assumed to be uniform over the entire conducting surface. If the cylinder has perfect conductivity, Z_{ij} is symmetric and CDANT sets up just the upper-right triangular portion of C(I,J). With finite conductivity, the entire square matrix is generated. If any segment has a length exceeding 0.477 λ, CDANT returns with C(I,J) = 0 and ISYM = 10.

C(I,J) denotes the mutual impedance between the electric test dipole I and expansion mode J. To calculate Z_{ij} from Eq. (10), we integrate over dipole J using the current $\underline{J}_j$ of dipole J and the field of dipole I. It is convenient to express Z_{ij} as the sum of an integral over segment JA(J) and an integral over segment JB(J). (These are the two segments of dipole J.) Furthermore, the field of dipole I is the sum of the fields from segments JA(I) and JB(I). Thus, Z_{ij} can be expressed as the sum of four double integrals:

$$(64) \qquad Z_{ij} = \frac{\eta}{4} \sum_L \sum_K \int_L \underline{J}_j \cdot \int_K [k \, \underline{J}_i \, H_0 - \hat{\rho} \, J_i' \, H_1] \, ds \, dt$$

where $\underline{J}_i$ is the current density of dipole I. Equation (64) follows from Eqs. (10) and (22) for a perfectly conducting cylinder. The argument of H_0 and H_1 is $k\rho$ where ρ is the distance between a source-point on segment K and a point on segment L, and $\hat{\rho}$ is the corresponding unit vector. The dipole current distributions $J_i(s)$ and $J_j(t)$ are sinusoidal as in Section IV and have unit value at the dipole terminals. From Eq. (64), it is convenient to consider the dipole-dipole impedance Z_{ij} to be the sum of four segment-segment impedances Z_{LK}.

CDANT selects a segment K (at statement 30) and another segment L. As in Eq. (64), K is a segment of test-dipole I and L is a segment of expansion mode J. The segment-segment impedance Z_{LK} is obtained by calling a subroutine. In statement 168, this impedance is then added to Z_{ij}.

In CDANT, segment K has endpoints KA and KB and segment L has endpoints LA and LB. It is convenient to think of KA and KB as points 1 and 2 on segment K, and LA and LB as points 1 and 2 on L. Now we can define four segment-segment impedances P(IS,JS). The first subscript IS refers to the terminal point on segment K, and the second subscript JS refers to the terminal point on L. Thus IS = 1 or 2 if dipole I has its terminal point I2(I) at KA (point 1) or KB (point 2), respectively. Similarly JS = 1 or 2 if mode J has its terminal point I2(J) at LA or LB, respectively. The impedances P(IS,JS) are defined with the following reference directions for current flow: from point 1 toward point 2 on each segment. If dipole I has this same reference direction on segment K we set FI = 1; otherwise FI = -1. Similarly, FJ = ±1 in accordance with the reference direction for mode J on segment L. In statement 168 P(IS,JS) is multiplied by FI and FJ before its contribution is added to Z_{ij}.

CDANT calls subroutine ZMM1 if the segment numbers K and L are identical, ZMM2 if segments K and L intersect, or ZMM3 otherwise. Subroutine ZMM2 calculates the impedances Q(KK,LL) which are like the P(IS,JS) but have different conventions on reference directions and subscript meaning. The transformation from the Q impedances to the P impedances is accomplished in statement 98.

```
      SUBROUTINE CDANT(C,D,X,Y,ZS,IA,IB,I1,I2,I3,ISYM
     2,IDM,INT,JA,JB,MD,N,ND,NM,NP)
      COMPLEX ZS,P11,P12,P21,P22,Q11,Q12,Q21,Q22,P(2,2),Q(2,2)
      COMPLEX C(IDM,IDM)
      DIMENSION X(IDM),Y(IDM),D(IDM),IA(IDM),IB(IDM),JA(IDM),JB(IDM)
      DIMENSION I1(IDM),I2(IDM),I3(IDM),MD(IDM,5),ND(IDM)
      DO 20 I=1,N
      DO 20 J=1,N
   20 C(I,J)=(.0,.0)
      DMAX=.0
      DO 25 J=1,NM
      DK=D(J)
   25 IF(DK.GT.DMAX)DMAX=DK
      IF(DMAX.LT.3.)GO TO 30
      ISYM=10
      RETURN
   30 DO 200 K=1,NM
      NDK=ND(K)
      KA=IA(K)
      KB=IB(K)
      DK=D(K)
      DO 200 L=1,NM
      NDL=ND(L)
      LA=IA(L)
      LB=IB(L)
      DL=D(L)
      NIL=0
```

Fig. 29. Subroutine CDANT.

```
      DO 200 II=1,NDK
      I=MD(K,II)
      FI=1.
      IF(KB.EQ.I2(I))GO TO 36
      IF(KB.EQ.I1(I))FI=-1.
      IS=1
      GO TO 40
   36 IF(KA.EQ.I3(I))FI=-1.
      IS=2
   40 DO 200 JJ=1,NDL
      J=MD(L,JJ)
      IF(ISYM.NE.0)GO TO 42
      IF(I.GT.J)GO TO 200
   42 FJ=1.
      IF(LB.EQ.I2(J))GO TO 46
      IF(LB.EQ.I1(J))FJ=-1.
      JS=1
      GO TO 50
   46 IF(LA.EQ.I3(J))FJ=-1.
      JS=2
   50 IF(NIL.NE.0)GO TO 168
      NIL=1
      IF(K.EQ.L)GO TO 120
      IND=(LA-KA)*(LB-KA)*(LA-KB)*(LB-KB)
      IF(IND.EQ.0)GO TO 80
C     SEGMENTS K AND L SHARE NO POINTS
      CALL ZMM3(X(KA),Y(KA),X(KB),Y(KB),X(LA),Y(LA),X(LB),Y(LB),ZS,
     2DK,DL,INT,P(1,1),P(1,2),P(2,1),P(2,2))
      GO TO 168
C     SEGMENTS K AND L SHARE ONE POINT (THEY INTERSECT)
   80 KG=3
      JM=KB
      JC=KA
      KF=-1
      IND=(KB-LA)*(KB-LB)
      IF(IND.NE.0)GO TO 82
      JC=KB
      KF=1
      JM=KA
      KG=0
   82 LG=3
      JP=LA
      LF=-1
      IF(LB.EQ.JC)GO TO 83
      JP=LB
      LF=1
      LG=0
   83 SGN=KF*LF
      CALL ZMM2(X(JM),Y(JM),X(JC),Y(JC),X(JP),Y(JP),ZS,DK,DL,
     2INT,Q(1,1),Q(1,2),Q(2,1),Q(2,2))
      DO 98 KK=1,2
      KP=IABS(KK-KG)
      DO 98 LL=1,2
      LP=IABS(LL-LG)
   98 P(KP,LP)=SGN*Q(KK,LL)
      GO TO 168
C     K=L  (SELF REACTION OF SEGMENT K)
  120 CALL ZMM1(DK,ZS,P(1,1),P(1,2))
      P(2,1)=P(1,2)
      P(2,2)=P(1,1)
  168 C(I,J)=C(I,J)+FI*FJ*P(IS,JS)
  200 CONTINUE
      RETURN
      END
```

Fig. 29. (Continued)

APPENDIX IV
Subroutine ZMM1

ZMM1, listed in Fig. 30, calculates the self-impedances of a sinusoidal strip monopole as defined in Appendix 3. (The terms "monopole" and "segment" are used interchangeably.) These impedances are obtained in functional form (as opposed to numerical integration) with the aid of Eq. (24) and the following:

$$(65)\quad k\int_0^h H_0(kx)\sin(kx)\,dx = 2j/\pi + kh\,[H_0(kh)\sin(kh) - H_1(kh)\cos(kh)]$$

$$(66)\quad k\int_0^h H_0(kx)\cos(kx)\,dx = kh\,[H_0(kh)\cos(kh) + H_1(kh)\sin(kh)]$$

where k and h are positive. Since $P_{21} = P_{12}$ and $P_{22} = P_{11}$, ZMM1 calculates only P_{11} and P_{12}.

The impedance contribution ΔP arising from finite conductivity is

$$(67)\quad \Delta P = \int \underline{M}_n \cdot \underline{H}_m \, d\ell = Z_s \int \underline{J}_n \cdot (\hat{n} \times \underline{H}_m)\, d\ell = \frac{Z_s}{2}\int \underline{J}_m \cdot \underline{J}_n \, d\ell$$

where the subscripts m and n refer to the test-source and the expansion mode, respectively. To explain the factor of one-half in the last form of Eq. (67), consider the free-space field of the test monopole. If the observer approaches the surface of the monopole, the field is $\underline{H}_m = \pm \hat{z}\, J_m/2$.

```
      SUBROUTINE ZMM1(DK,ZS,P11,P12)
      COMPLEX ZS,H0,H1,P11,P12
      DATA PI/3.14159/
      CDK=COS(DK)
      SDK=SIN(DK)
      CALL HANK(DK,H0,H1,2)
      SDKS=SDK**2
      CDKS=CDK**2
      P11 =-2.*H1*CDK+H0*SDK+2.*(.0,1.)*(1.+CDKS)/PI/DK
      P12 =-H0*CDK*SDK+H1*(1.+CDKS)-4.*(.0,1.)*CDK/PI/DK
      P11=15.*DK*P11/SDKS
      P12=15.*DK*P12/SDKS
      RS=REAL(ZS)
      IF(RS.LE.0.)GO TO 100
      CST=16.*PI*SDKS
      TDK=2.*DK
      CTDK=COS(TDK)
      STDK=SIN(TDK)
      P11=P11+ZS*(TDK-STDK)/CST
      P12 =P12 +ZS*((1.-CTDK)*SDK+(STDK-TDK)*CDK)/CST
  100 CONTINUE
      RETURN
      END
```

Fig. 30. Subroutine ZMM1.

APPENDIX V
Subroutine ZMM2

Subroutine ZMM2, listed in Fig. 31, calculates the segment-segment impedances of two intersecting strip monopoles. The input data are:

X1, Y1	Coordinates (kx_1, ky_1) of the free end of the source segment
X2, Y2	Coordinates of the point of intersection
X3, Y3	Coordinates of the free end of segment 2
DK1	Length kh_1 of source segment
DK2	Length kh_2 of segment 2.

Figure 32 illustrates the intersecting segments after a coordinate rotation and translation. Point 1 is at the origin and point 2 lies on the positive x axis at $x = h_1$. The new coordinates of point 3 are denoted by XB and YB. Segment 1 lies on the x axis and α denotes the angle between segment 2 and the x axis. AL, CAL and SAL denote α, $\cos\alpha$ and $\sin\alpha$. If α vanishes, the two segments are coplanar. In this event, the impedances are calculated in closed form just above Statement 20. In the coplanar situation the magnetic field of segment 1 vanishes over segment 2 and there is no coupling via the surface impedance.

Figure 32 shows the reference directions for the current density $\underline{J}$ as used in the definition of the impedances Q11, Q12, Q21 and Q22. Figure 32 also shows the endpoint numbering system for segments 1 and 2 as used in defining these impedances. As usual, the first and second subscripts on Q indicate the terminal points on segments 1 and 2, respectively.

If the cylinder has perfect conductivity, the mutual impedance between monopoles 1 and 2 is

$$(68)\quad Z = -\int_0^{h_2} \underline{J}_2(t)\cdot\underline{E}_1(t)\,dt$$

where $\underline{J}_2$ is the expansion-mode current density on monopole 2 and $\underline{E}_1$ is the free-space field of monopole 1. Coordinate t denotes the distance from the junction to an arbitrary point on segment 2.

Let E_x and E_y denote the components of $\underline{E}_1$. It is convenient to let $Z = Z_x + Z_y$ where

$$(69)\quad Z_x = -\cos(\alpha) \int J(t)\, E_x(t)\, dt$$

$$(70)\quad Z_y = -\sin(\alpha) \int J(t)\, E_y(t)\, dt$$

ZMM2 uses Eq. (24) for E_x. Comparison of Figs. 3 and 32 shows that $\rho_2 = t$. Thus, one term in Z_x can be integrated in closed form via Eqs. (65) and (66). This is accomplished immediately after statement 20, and the result is denoted by S11, S12, etc. The remaining term in Z_x requires the integration of $J(t)\, H_0(k\rho_1)$. This is evaluated with Simpson's rule in the DO LOOP ending at statement 90, and the result is immediately lumped into S11, S12, etc.

We still have to calculate Z_y and the impedance contribution ΔZ from the surface impedance ZS. For Z_y we obtain E_y from the second integral in Eq. (22). For ΔZ we use the first expression in Eq. (10) and $\underline{H}$ from Eq. (16). Both Z_y and ΔZ have the following form:

$$(71)\quad R = \sin(\alpha) \int_0^{h_2} \int_0^{h_1} F_1(s)\, J_2(t)\, (t/\rho)\, H_1(k\rho)\, ds\, dt$$

where

$$(72)\quad \rho^2 = s^2 + 2st\cos(\alpha) + t^2$$

and $F_1(s)$ represents $J_1(s)$ or $J_1'(s)$. Coordinate s denotes the distance from the junction to an arbitrary point on segment 1. In Eq. (71) the integrand is singular at $(s,t) = (0,0)$. To remove the singularity, we make three successive changes of variable as follows:

$$(73)\quad p = (t + s)/\sqrt{2} \qquad q = (t - s)/\sqrt{2}$$

$$(74)\quad u = \sqrt{2}\, p \cos(\alpha/2) \qquad v = \sqrt{2}\, q \sin(\alpha/2)$$

$$(75)\quad u = \rho\cos\phi \qquad v = \rho\sin\phi.$$

In the final transformation (Eq. (75)), the integration variable ϕ should not be confused with the angle ϕ shown in Fig. 3. From Eqs. (71)-(75),

$$(76)\quad s = \rho\,\frac{\sin(\alpha/2 - \phi)}{\sin\alpha} \qquad t = \rho\,\frac{\sin(\alpha/2 + \phi)}{\sin\alpha}$$

$$(77)\quad R = \int_{-\alpha/2}^{\alpha/2} \int_{0}^{\rho_m} F_1(s)\, J_2(t)\, t\, H_1(k\rho)\, d\rho\, d\phi$$

$$(78)\quad \rho_m = \frac{h_1 \sin(\alpha)}{\sin(\alpha/2 - \phi)}, \qquad \phi \leq \phi_o$$

$$(79)\quad \rho_m = \frac{h_2 \sin(\alpha)}{\sin(\alpha/2 + \phi)}, \qquad \phi \geq \phi_o$$

$$(80)\quad \tan\phi_o = \frac{(h_2 - h_1)\tan(\alpha/2)}{h_2 + h_1} \quad .$$

ZMM2 evaluates Eq. (77) with Simpson's rule. The ρ integration is performed in the DO LOOP ending at statement 100, and the ϕ integration is in the outer DO LOOP ending at statement 200.

```
      SUBROUTINE ZMM2(X1,Y1,X2,Y2,X3,Y3,ZS
     2,DK1,DK2,INT,Q11,Q12,Q21,Q22)
      COMPLEX H0,H1,HH0,HH1,SH0,SH1,Q11,Q12,Q21,Q22
      COMPLEX DHH0,DHH1,DH0,DH1,DSH0,DSH1
      COMPLEX S11,S12,S21,S22,T11,T12,T21,T22,Y11,Y12,Y21,Y22
      COMPLEX DT11,DT12,DT21,DT22,DY11,DY12,DY21,DY22
      COMPLEX ZS,RKH1,SX1,SX2,CCP,FUN,CQT
      DATA CCP/(.0,.63662)/
      DATA PI/3.14159/
      SDK1=SIN(DK1)
      SDK2=SIN(DK2)
      CDK1=COS(DK1)
      CDK2=COS(DK2)
      CBET=(X2-X1)/DK1
      SBET=(Y2-Y1)/DK1
      XB=(X3-X1)*CBET+(Y3-Y1)*SBET
      YB=-(X3-X1)*SBET+(Y3-Y1)*CBET
      CAL=(XB-DK1)/DK2
      SAL=ABS(YB/DK2)
      CALL HANK(DK2,HH0,HH1,2)
      DHH0=DK2*HH0
      DHH1=DK2*HH1
      C1S2=CDK1*SDK2
      C1C2=CDK1*CDK2
      IF(CAL.LT.0.)GO TO 20
      IF(SAL.GT..04)GO TO 20
      CNT=-15.*CAL/SDK1/SDK2
      CALL HANK(DK1,H0,H1,2)
      DH0=DK1*H0
      DH1=DK1*H1
      DKS=DK1+DK2
      CALL HANK(DKS,SH0,SH1,2)
      DSH0=DKS*SH0
      DSH1=DKS*SH1
      Q11=CNT*(CDK1*DSH1-C1S2*DH0-C1C2*DH1-DHH1+CCP*CDK2)
      Q12=CNT*(CDK2*DHH1-SDK2*DHH0-CCP+CDK1*DH1+C1S2*DSH0-C1C2*DSH1)
      Q21=CNT*(SDK2*DH0-DSH1+CDK2*DH1+CDK1*DHH1-CCP*C1C2)
      Q22=CNT*(C1S2*DHH0-C1C2*DHH1+CCP*CDK1-DH1-SDK2*DSH0+CDK2*DSH1)
      RETURN
20    CONTINUE
      S11=-DHH1+CCP*CDK2
      S12=-SDK2*DHH0+CDK2*DHH1-CCP
      S21=(DHH1-CCP*CDK2)*CDK1
      S22=(SDK2*DHH0-CDK2*DHH1+CCP)*CDK1
      DKS1=DK1**2
      AL=ATAN2(SAL,CAL)
      RMIN=DK1
      IF(CAL.GE.0.)GO TO 30
      RMIN=DK1*SAL
      DCR=-DK1*CAL
      IF(DK2.LT.DCR)RMIN=SQRT(DKS1+2.*DK1*DK2*CAL+DK2*DK2)
30    ENT=1+(4*INT)/10
      INP=ENT*DK2/RMIN
      INP=2*(INP/2)
      IF(INP.LT.2)INP=2
      FIT=INP
      IP=INP+1
      DT=DK2/FIT
      TK=.0
      SX1=(.0,.0)
      SX2=(.0,.0)
      SGI=-1.
```

Fig. 31. Subroutine ZMM2.

```
      DO 90 I=1,IP
      D=SGI+3.
      IF(I.EQ.1)D=1.
      IF(I.EQ.IP)D=1.
      TKS=TK*TK
      RK=SQRT(DKS1+2.*DK1*TK*CAL+TKS)
      CALL HANK(RK,H0,H1,0)
      S1=SIN(DK2-TK)
      S2=SIN(TK)
      SX1=SX1+S1*H0*D
      SX2=SX2+S2*H0*D
      SGI=-SGI
      TK=TK+DT
   90 CONTINUE
      SX1=SX1*DT/3.
      SX2=SX2*DT/3.
      S21=S21-SX1
      S22=S22-SX2
      S12=S12+CDK1*SX2
      S11=S11+CDK1*SX1
      INP=2*(INT/2)
      IP=INP+1
      FIT=INP
      JP=IP
      T11=(.0,.0)
      T12=(.0,.0)
      T21=(.0,.0)
      T22=(.0,.0)
      COT=(.0,.0)
      RS=REAL(ZS)
      Y11=(.0,.0)
      Y12=(.0,.0)
      Y21=(.0,.0)
      Y22=(.0,.0)
      B=.0
      IF(AL.LT..05)GO TO 210
      ALT=AL/2.
      CALT=COS(ALT)
      SALT=SIN(ALT)
      RCP=(DK1+DK2)*CALT
      RSP=(DK2-DK1)*SALT
      PHC=ATAN2(RSP,RCP)
      SGI=-1.
      PH=-ALT
      DPH=AL/FIT
      DO 200 I=1,IP
      D=SGI+3.
      IF(I.EQ.1)D=1.
      IF(I.EQ.IP)D=1.
      SAP=SIN(ALT+PH)
      SAM=SIN(ALT-PH)
      IF(PH.LE.PHC)RMAX=DK1*SAL/SAM
      IF(PH.GT.PHC)RMAX=DK2*SAL/SAP
      DRK=RMAX/FIT
      RK=.0
      SGJ=-1.
      DT11=(.0,.0)
      DT12=(.0,.0)
      DT21=(.0,.0)
      DT22=(.0,.0)
      DY11=(.0,.0)
      DY12=(.0,.0)
```

Fig. 31. (Continued)

```
      DY21=(.0,.0)
      DY22=(.0,.0)
      RKH1=CCP
      DO 100 J=1,JP
      C=SGJ+3.
      IF(J.EQ.1)C=1.
      IF(J.EQ.JP)C=1.
      IF(J.EQ.1)GO TO 94
      CALL HANK(RK,H0,H1,1)
      RKH1=RK*H1
   94 CONTINUE
      SK=RK*SAM/SAL
      TK=RK*SAP/SAL
      C1=COS(SK)
      C2=COS(DK1-SK)
      S1=SIN(DK2-TK)
      S2=SIN(TK)
      FUN=C*RKH1
      DY11=DY11-FUN*C1*S1
      DY12=DY12-FUN*C1*S2
      DY21=DY21+FUN*C2*S1
      DY22=DY22+FUN*C2*S2
      SGJ=-SGJ
      RK=RK+DRK
      IF(RS.LE.0.)GO TO 100
      SS1=SIN(SK)
      SS2=SIN(DK1-SK)
      DT11=DT11+FUN*SS1*S1
      DT12=DT12+FUN*SS1*S2
      DT21=DT21+FUN*SS2*S1
      DT22=DT22+FUN*SS2*S2
  100 CONTINUE
      B=SAP*DRK*D
      Y11=Y11+B*DY11
      Y12=Y12+B*DY12
      Y21=Y21+B*DY21
      Y22=Y22+B*DY22
      PH=PH+DPH
      SGI=-SGI
      IF(RS.LE.0.)GO TO 200
      T11=T11+B*DT11
      T12=T12+B*DT12
      T21=T21+B*DT21
      T22=T22+B*DT22
  200 CONTINUE
      B=DPH/9.
      IF(RS.GT.0.)CQT=(.0,1.)*ZS*DPH/(72.*PI*SDK1*SDK2*SAL)
  210 CONTINUE
      CNT=-15./SDK1/SDK2
      Q11=CNT*(CAL*S11+B*Y11)+CQT*T11
      Q12=CNT*(CAL*S12+B*Y12)+CQT*T12
      Q21=CNT*(CAL*S21+B*Y21)+CQT*T21
      Q22=CNT*(CAL*S22+B*Y22)+CQT*T22
      RETURN
      END
```

Fig. 31. (Continued)

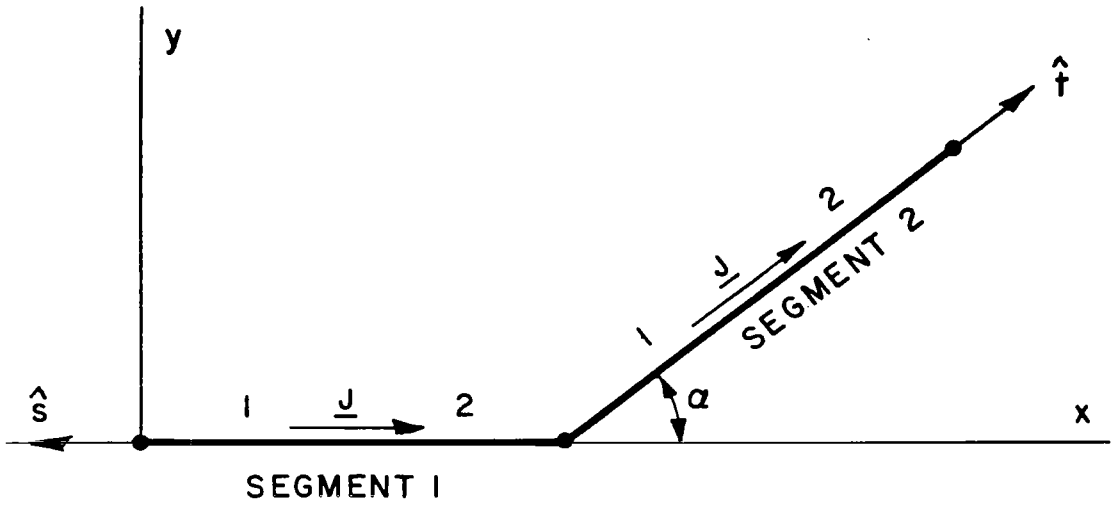

Fig. 32. Intersecting segments in ZMM2.

APPENDIX VI
Subroutine ZMM3

ZMM3, listed in Fig. 33, calculates the mutual impedances P11, P12, P21 and P22 of two spatially-separated monopoles. In the input data (X1,Y1) and (X2,Y2) are the coordinates of the endpoints of segment 1. For example, X1 = kx_1. Similarly, (X3,Y3) and (X4,Y4) are the endpoints of segment 2. DK1 and DK2 denote the segment lengths kh_1 and kh_2.

A coordinate rotation and translation is applied to move segment 1 onto the x axis with (X1,Y1) at the origin and (X2,Y2) at (x,y) = (DK1,0). The new coordinates of (X3,Y3) and (X4,Y4) are denoted by (XA,YA) and (XB,YB), respectively. Now segment 2 forms an angle α with the x axis, and CAL and SAL denote $\cos(\alpha)$ and $\sin(\alpha)$. RMIN denotes the shortest distance between segment 1 and segment 2 and is employed to determine the number of terms in the numerical integrations.

In the DO LOOP ending at statement 50, a trigonometric table is calculated and stored. These sine and cosine functions represent the modal current (and its derivative) on segment 1. These are multiplied by the Simpson-rule integration coefficients before storing.

If the cylinder has perfect conductivity, the impedance is given by Eqs. (68), (69) and (70). We use Eq. (24) for E_x in Eq. (69). To obtain E_y for Eq. (70), we use a component from the second integral in Eq. (22). To obtain H_z for the surface-impedance term ΔZ, we use Eq. (16).

The DO LOOP ending with statement 100 uses Simpson's rule to integrate over segment 1 in the calculation of E_y and H_z. The outer DO LOOP ending with statement 200 uses Simpson's rule to integrate $\underline{J}_2 \cdot \underline{E}_1$ and $J_2 H_1$ over segment 2. The impedance Z of the perfectly conducting cylinder is denoted by S11, S12, etc. The term ΔZ is denoted by T11, T12, etc.

```
      SUBROUTINE ZMM3(X1,Y1,X2,Y2,X3,Y3,X4,Y4,ZS,
     2DK1,DK2,INT,P11,P12,P21,P22)
      COMPLEX HHA,HHB,ZS,HZ1,HZ2,COT,ET1,ET2,H0,H1
      COMPLEX P11,P12,P21,P22,S11,S12,S21,S22,T11,T12,T21,T22
      DIMENSION CC1(21),SS1(21),CC2(21),SS2(21)
      DATA ETA,PI/376.727,3.14159/
      S11=(.0,.0)
      S12=(.0,.0)
      S21=(.0,.0)
      S22=(.0,.0)
      T11=(.0,.0)
      T12=(.0,.0)
      T21=(.0,.0)
      T22=(.0,.0)
      CBET=(X2-X1)/DK1
      SBET=(Y2-Y1)/DK1
      XA=(X3-X1)*CBET+(Y3-Y1)*SBET
      XB=(X4-X1)*CBET+(Y4-Y1)*SBET
      YA=-(X3-X1)*SBET+(Y3-Y1)*CBET
      YB=-(X4-X1)*SBET+(Y4-Y1)*CBET
      CAL=(XB-XA)/DK2
      SAL=(YB-YA)/DK2
      RMIN=10000.
      X=XA
      Y=YA
      DX=DK2*CAL/4.
      DY=DK2*SAL/4.
      DO 40 J=1,5
      YS=.0
      R=ABS(Y)
      IF(R.GT.1.E-15)YS=Y*Y
      XS=.0
      XAB=ABS(X-DK1)
      IF(XAB.GT.1.E-15)XS=XAB*XAB
      IF(X.LT.0.)R=SQRT(X*X+YS)
      IF(X.GT.DK1)R=SQRT(XS+YS)
      IF(R.LT.RMIN)RMIN=R
      X=X+DX
      Y=Y+DY
   40 CONTINUE
      ENT=1+(4*INT)/10
      ISS=ENT*DK1/RMIN
      ISS=2*(ISS/2)
      IF(ISS.LT.2)ISS=2
      IF(ISS.GT.20)ISS=20
      FSS=ISS
      ISQ=ISS+1
      DS=DK1/FSS
      ITT=ENT*DK2/RMIN
      ITT=2*(ITT/2)
      IF(ITT.LT.2)ITT=2
      IF(ITT.GT.20)ITT=20
      FTT=ITT
      ITQ=ITT+1
      DT=DK2/FTT
      XP=.0
      SGN=-1.
      RS=REAL(ZS)
      JUMP=0
      ASAL=ABS(SAL)
      IF(RS.LE.0..AND.ASAL.LT..04)JUMP=1
      IF(JUMP.EQ.1)GO TO 60
```

Fig. 33. Subroutine ZMM3.

```
      DO 50 I=1,ISQ
      C=SGN+3.
      IF(I.EQ.1)C=1.
      IF(I.EQ.ISQ)C=1.
      CC1(I)=C*COS(DK1-XP)
      SS1(I)=C*SIN(DK1-XP)
      CC2(I)=C*COS(XP)
      SS2(I)=C*SIN(XP)
      SGN=-SGN
      XP=XP+DS
   50 CONTINUE
   60 CONTINUE
      DX=DT*CAL
      DY=DT*SAL
      X=XA
      Y=YA
      TK=.0
      SGJ=-1.
      CDK1=COS(DK1)
      DO 200 J=1,ITQ
      D=SGJ+3.
      IF(J.EQ.1)D=1.
      IF(J.EQ.ITQ)D=1.
      CT1=D*SIN(DK2-TK)
      CT2=D*SIN(TK)
      XP=.0
      YS=.0
      YAB=ABS(Y)
      IF(YAB.GT.1.E-15)YS=YAB*YAB
      ET1=(.0,.0)
      ET2=(.0,.0)
      HZ1=(.0,.0)
      HZ2=(.0,.0)
      RKA=SQRT(X*X+YS)
      RKB=SQRT((X-DK1)**2+YS)
      SPH=YAB/RKA+YAB/RKB
      IF(SPH.LT..04)GO TO 110
      IF(JUMP.EQ.1)GO TO 110
      DO 100 I=1,ISQ
      DELX=ABS(X-XP)
      DXS=.0
      IF(DELX.GT.1.E-15)DXS=DELX*DELX
      RK=SQRT(DXS+YS)
      SPH=Y/RK
      C1=CC1(I)
      S1=SS1(I)
      C2=CC2(I)
      S2=SS2(I)
      CALL HANK(RK,H0,H1,1)
      ET1=ET1-C1*SPH*H1
      ET2=ET2+C2*SPH*H1
      XP=XP+DS
      IF(PS.LE.0.)GO TO 100
      HZ1=HZ1+S1*H1*SPH
      HZ2=HZ2+S2*H1*SPH
  100 CONTINUE
  110 CONTINUE
      CALL HANK(RKA,HHA,H1,0)
      CALL HANK(RKB,H0,H1,0)
      ET1=ET1*SAL*DS/3.+CAL*(CDK1*HHA-H0)
      ET2=ET2*SAL*DS/3.+CAL*(CDK1*H0-HHA)
      S11=S11+CT1*ET1
```

Fig. 33. (Continued)

```
      S12=S12+CT2*ET1
      S21=S21+CT1*ET2
      S22=S22+CT2*ET2
      SGJ=-SGJ
      TK=TK+DT
      X=X+DX
      Y=Y+DY
      IF(RS.LE.0.)GO TO 200
      T11=T11+CT1*HZ1
      T12=T12+CT2*HZ1
      T21=T21+CT1*HZ2
      T22=T22+CT2*HZ2
  200 CONTINUE
      SDK1=SIN(DK1)
      SDK2=SIN(DK2)
      CST=-ETA*DT/(24.*PI*SDK1*SDK2)
      CQT=(.0,1.)*DS*DT*ZS/(72.*PI*SDK1*SDK2)
      P11=CST*S11+CQT*T11
      P12=CST*S12+CQT*T12
      P21=CST*S21+CQT*T21
      P22=CST*S22+CQT*T22
      RETURN
      END
```

Fig. 33. (Continued)

APPENDIX VII
Subroutine HANK

HANK, listed in Fig. 34, generates the Hankel functions of the second kind $H_0(x)$ and $H_1(x)$ denoted by H and H1. The input data are the argument X and the integer ID. Although ID is ignored in HANK, it is defined as follows: Let ID = 0, 1 or 2 if H_0, H_1 or both are required.

HANK always generates H_0 and H_1 on each call. An improvement in computational speed could be achieved by generating just the required function as indicated by ID.

In this subroutine B and B1 denote the Bessel functions and Y and Y1 the Neumann functions. HANK uses the polynomial approximations given in reference [17].

```
      SUBROUTINE HANK(X,H,H1,ID)
      COMPLEX H,H1
      DATA TSP/.636619772/
      IF(X.GT.3.)GO TO 100
      XLN=TSP*ALOG(X/2.)
      B=.0
      B1=.0
      Y=.0
      Y1=.0
      X1=X/3.
      X2=X1*X1
      IF(X1.LT..1)GO TO 60
      X4=X2*X2
      X6=X2*X4
      IF(X1.LT..3)GO TO 55
      X8=X2*X6
      X10=X2*X8
      X12=X2*X10
      B=.21E-3*X12-.39444E-2*X10+.444479E-1*X8
      Y=-.24846E-3*X12+.427916E-2*X10-.4261214E-1*X8
      B1=.1109E-4*X12-.31761E-3*X10+.443319E-2*X8
      Y1=.27873E-2*X12-.400976E-1*X10+.3123951*X8
55    B=B-.3163866*X6+1.2656208*X4
      Y=Y+.25300117*X6-.74350384*X4
      B1=B1-.3954289E-1*X6+.21093573*X4
      Y1=Y1-1.3164827*X6+2.1682709*X4
60    B=B-2.2499997*X2+1.
      Y=Y+.60559366*X2+.36746691+XLN*B
      B1=X*(B1-.56249985*X2+.5)
      Y1=(Y1+.2212091*X2-.6366198)/X+XLN*B1
      GO TO 200
100   SW=SQRT(X)
      X1=3./X
      X2=X1*X1
      X3=X1*X2
      X4=X1*X3
      X5=X1*X4
      X6=X1*X5
      F=.79788456-.77E-6*X1-.55274E-2*X2-.9512E-4*X3+.137237E-2*X4
     2-.72805E-3*X5+.14476E-3*X6
      T=X-.78539816-.4166397E-1*X1-.3954E-4*X2+.262573E-2*X3
     2-.54125E-3*X4-.29333E-3*X5+.13558E-3*X6
      B=F*COS(T)/SW
      Y=F*SIN(T)/SW
      F=.79788456+.156E-5*X1+.1659667E-1*X2+.17105E-3*X3-.249511E-2*X4
     2+.113653E-2*X5-.20033E-3*X6
      T=X-2.3561945+.12499612*X1+.565E-4*X2-.637879E-2*X3+.74348E-3*X4
     2+.79824E-3*X5-.29166E-3*X6
      B1=F*COS(T)/SW
      Y1=F*SIN(T)/SW
200   H=CMPLX(B,-Y)
      H1=CMPLX(B1,-Y1)
      RETURN
      END
```

Fig. 34. Subroutine HANK.

APPENDIX VIII
Subroutine CROUT

CROUT, listed in Fig. 35, solves a system of simultaneous linear equations with complex coefficients. This subroutine uses the method of P. D. Crout described in Reference [18]. Although this subroutine does not use pivoting, it is efficient and accurate in the application discussed herein. The input data are defined as follows:

C(I,J)	Complex coefficients in the simultaneous equations
S(I)	Excitation column
N	Size of the square matrix C
IDM	Dimensions of C and S
ISYM	Zero or one for symmetric or nonsymmetric matrix
IWR	One or zero to write or suppress the solution
I12	One or two if C is original or auxiliary matrix.

If I12 = 1, CROUT will convert the original matrix C into the auxiliary matrix. The auxiliary matrix is overlaid in the same location C, wiping out the original matrix. Similarly, the solution is stored in S(I) which contained the excitation column. Of course, N must not exceed IDM. If IWR = 1, the solution will be printed out with the following definitions:

I	Index number of the solution S(I)
SNOR	Normalized magnitude of S(I)
SA	Absolute magnitude of S(I)
PH	Phase of S(I) in degrees.

```
      SUBROUTINE CROUT(C,S,N,IDM,ISYM,IWR,I12)
      COMPLEX C(IDM,IDM),S(IDM)
      COMPLEX F,P,SS,T
2     FORMAT(1X,1I5,1F10.3,1F15.7,1F10.0)
5     FORMAT(1HO)
      IF(I12.NE.1)GO TO 22
      IF(N.EQ.1)S(1)=S(1)/C(1,1)
      IF(N.EQ.1)GO TO 100
      IF(ISYM.NE.0)GO TO 8
      DO 6 I=1,N
      DO 6 J=I,N
      C(J,I)=C(I,J)
6     CONTINUE
8     CONTINUE
      F=C(1,1)
      DO 10 L=2,N
```

Fig. 35. Subroutine CROUT.

```
10   C(1,L)=C(1,L)/F
     DO 20 L=2,N
     LLL=L-1
     DO 20 I=L,N
     F=C(I,L)
     DO 11 K=1,LLL
11   F=F-C(I,K)*C(K,L)
     C(I,L)=F
     IF(L.EQ.I)GO TO 20
     P=C(L,L)
     IF(ISYM.EQ.0)GO TO 15
     F=C(L,I)
     DO 12 K=1,LLL
12   F=F-C(L,K)*C(K,I)
     C(L,I)=F/P
     GO TO 20
15   F=C(I,L)
     C(L,I)=F/P
20   CONTINUE
22   CONTINUE
     DO 30 L=1,N
     P=C(L,L)
     T=S(L)
     IF(L.EQ.1)GO TO 30
     LLL=L-1
     DO 25 K=1,LLL
25   T=T-C(L,K)*S(K)
30   S(L)=T/P
     DO 38 L=2,N
     I=N-L+1
     II=I+1
     T=S(I)
     DO 35 K=II,N
35   T=T-C(I,K)*S(K)
38   S(I)=T
     IF(IWR.LE.0) GO TO 100
     CNOR=.0
     DO 40 I=1,N
     SA=CABS(S(I))
     IF(SA.GT.CNOR)CNOR=SA
40   CONTINUE
     IF(CNOR.LE.0.)CNOR=1.
     DO 44 I=1,N
     SS=S(I)
     SA=CABS(SS)
     SNOR=SA/CNOR
     PH=.0
     IF(SA.GT.0.)PH=57.29578*ATAN2(AIMAG(SS),REAL(SS))
     WRITE(6,2)I,SNOR,SA,PH
44   CONTINUE
     WRITE(6,5)
100  CONTINUE
     RETURN
     END
```

Fig. 35. (Continued)

APPENDIX IX
Subroutine VNAS

VNAS, listed in Fig. 36, arranges the solution for a two-sided narrow axial slot. The excitation column CJ(I) is set up to represent a unit voltage generator at the terminals of mode IGN. The current distribution induced on the cylinder is obtained by calling CROUT. The slot admittance Y11 is then equal to the current CJ(IGN) at the terminals.

```
      SUBROUTINE VNAS(IDM,IGN,ISYM,IWR,I12,N,C,CJ,Y11)
      COMPLEX C(IDM,IDM),CJ(IDM),Y11
      DO 20 I=1,N
20    CJ(I)=(.0,.0)
      CJ(IGN)=(1.,0.)
      CALL CROUT(C,CJ,N,IDM,ISYM,IWR,I12)
      I12=2
      Y11=CJ(IGN)
      RETURN
      END
```

Fig. 36. Subroutine VNAS.

APPENDIX X
Subroutine VWAS

VWAS, listed in Fig. 37, arranges the solution for a two-sided wide axial slot. AK denotes ka, where "a" is the aperture width. Most of the subroutine is concerned with generating the excitation column VJ(I) corresponding to a unit aperture voltage. A minor generalization of Eq. (38) is employed so that the aperture segments need not have equal lengths. The current distribution CJ(I) induced on the cylinder is obtained by calling CROUT. Finally the slot admittance Y11 is calculated as in Eq. (40).

```
      SUBROUTINE VWAS(IA,IB,IDM,ISYM,IWR,I1,I2,I3,I12,JSA,JSB,MD,N,ND
     2,NM,C,CJ,D,VJ,Y11)
      COMPLEX C(IDM,IDM),CJ(IDM),VJ(IDM),Y11
      DIMENSION IA(IDM),IB(IDM),I1(IDM),I2(IDM),I3(IDM),MD(IDM,5)
     2,ND(IDM),D(IDM)
      AK=.0
      DO 20 K=JSA,JSB
20    AK=AK+D(K)
      DO 30 I=1,N
30    VJ(I)=(.0,.0)
      IF(JSB.GT.JSA)GO TO 200
      K=JSA
      DK=D(K)
      V=(1.-COS(DK))/(AK*SIN(DK))
      KA=IA(K)
      KB=IB(K)
      NDK=ND(K)
      DO 140 II=1,NDK
      I=MD(K,II)
      FI=1.
      IF(KB.EQ.I2(I))GO TO 136
      IF(KB.EQ.I1(I))FI=-1.
      GO TO 140
136   IF(KA.EQ.I3(I))FI=-1.
140   VJ(I)=VJ(I)+FI*V
      GO TO 280
200   CONTINUE
      KA=IA(JSA)
      KB=IB(JSA)
      LA=IA(JSA+1)
      LB=IB(JSA+1)
      IND=(LA-KB)*(LB-KB)
      IF(IND.EQ.0)GO TO 210
      KA=IB(JSA)
      KB=IA(JSA)
```

Fig. 37. Subroutine VWAS.

```
210 CONTINUE
    DO 250 K=JSA,JSB
    DK=D(K)
    V=(1.-COS(DK))/(AK*SIN(DK))
    NDK=ND(K)
    DO 240 II=1,NDK
    I=MD(K,II)
    FI=1.
    IF(KB.EQ.I2(I))GO TO 236
    IF(KB.EQ.I1(I))FI=-1.
    GO TO 240
236 IF(KA.EQ.I3(I))FI=-1.
240 VJ(I)=VJ(I)+FI*V
    IF(K.EQ.JSB)GO TO 250
    LA=IA(K+1)
    LB=IB(K+1)
    KA=KB
    KB=LA
    IF(LA.EQ.KA)KB=LB
250 CONTINUE
280 CONTINUE
    DO 300 I=1,N
300 CJ(I)=VJ(I)
    CALL CROUT(C,CJ,N,IDM,ISYM,IWR,I12)
    I12=2
    Y11=(.0,.0)
    DO 400 I=1,N
400 Y11=Y11+VJ(I)*CJ(I)
    RETURN
    END
```

Fig. 37. (Continued)

APPENDIX XI
Subroutine VMLS

VMLS, listed in Fig. 38, arranges the solution for a parallel magnetic line source near a cylinder. Most of the subroutine is concerned with generating the excitation column for a one-volt magnetic line source. The integrations in Eq. (31) are performed in CMLS. The current distribution CJ(I) induced on the cylinder is obtained by calling CROUT. Finally the admittance Y11 of the line source is calculated.

```
      SUBROUTINE VMLS(IA,IB,IDM,INT,ISYM,IWR,I1,I2,I3,I12,MD,N,ND,NM,
     2C,CJ,D,PSI,VJ,X,Y,XS,YS,Y11,ZS)
      COMPLEX C(IDM,IDM),CJ(IDM),VJ(IDM),Y11,P1,P2,Q1,Q2,ZS
      DIMENSION IA(IDM),IB(IDM),I1(IDM),I2(IDM),I3(IDM)
      DIMENSION MD(IDM,5),ND(IDM),X(IDM),Y(IDM),D(IDM)
      DATA ETA,TP/376.727,6.28318/
      DO 100 I=1,N
      VJ(I)=(.0,.0)
  100 CJ(I)=(.0,.0)
      DO 240 K=1,NM
      KA=IA(K)
      KB=IB(K)
      CALL CMLS(PSI,X(KA),Y(KA),X(KB),Y(KB),XS,YS,D(K),INT,P1,P2,Q1,Q2)
      Q1=ZS*Q1
      Q2=ZS*Q2
      NDK=ND(K)
      DO 240 II=1,NDK
      I=MD(K,II)
      FI=1.
      IF(KB.EQ.I2(I)) GO TO 236
      IF(KB.EQ.I1(I)) FI=-1.
      CJ(I)=CJ(I)+FI*P1
      VJ(I)=VJ(I)+FI*(P1+Q1)
      GO TO 240
  236 IF(KA.EQ.I3(I)) FI=-1.
      CJ(I)=CJ(I)+FI*P2
      VJ(I)=VJ(I)+FI*(P2+Q2)
  240 CONTINUE
      CALL CROUT(C,CJ,N,IDM,ISYM,IWR,I12)
      I12=2
      Y11=CMPLX(TP/(4.*ETA),0.)
      DO 300 I=1,N
  300 Y11=Y11+CJ(I)*VJ(I)
      RETURN
      END
```

Fig. 38. Subroutine VMLS.

APPENDIX XII
Subroutine CMLS

CMLS, listed in Fig. 39, evaluates the coupling between a one-volt magnetic line source and an electric strip monopole. The line source has coordinates XS and YS. The monopole (or segment) has length DK and endpoint coordinates (X1,Y1) and (X2,Y2). P1 is the coupling to the mode with terminals at point 1, and P2 applies to terminals at point 2. The excitation voltage V_m in Eq. (31) is obtained by integrating over both segments of test-dipole m. CMLS integrates over one segment to obtain P1 and P2, and VMLS adds the appropriate quantities (P1 or P2) from two segments to obtain V_m.

D1 and D2 are the distances between the line source and (X1,Y1) and (X2,Y2) respectively. RMIN is the shortest distance between the line source and the segment.

A coordinate rotation and translation moves the segment onto the x axis with (X1,Y1) at the origin and (X2,Y2) at x = DK. The new coordinates of the line source are (XA,YA). The integration in Eq. (31) is evaluated with the trapezoidal rule in the DO LOOP ending at statement 100. Eq. (41) is employed for the electric field of the magnetic line source.

The admittance of a one-volt magnetic line source near a cylinder is defined as the magnetic field intensity H_z at the line source. The field H_z is the sum of the free-space field of the line source, the field H_z^J of the electric current on the cylinder, and the field H_z^M of the magnetic current on the cyliner.

By reciprocity, P1 and P2 are useful not only in generating the excitation column but also in calculating H_z^J. To permit VMLS to calculate the line-source admittance, CMLS also generates Q1 and Q2 which denote the field H_z^M from the magnetic current on one segment of the cylinder. Equations (6) and (42) are employed here, and the integrations for Q1 and Q2 are performed in the DO LOOP ending with statement 100.

```
      SUBROUTINE CMLS(PSI,X1,Y1,X2,Y2,XS,YS,DK,INT,P1,P2,Q1,Q2)
      COMPLEX CST,H0,H1,P1,P2,Q1,Q2
      DATA ETA/376.727/
      DKH=DK/25.
      D1=SQRT((XS-X1)**2+(YS-Y1)**2)
      D2=SQRT((XS-X2)**2+(YS-Y2)**2)
      P2=(.0,.0)
      P1=CMPLX(.5*PSI/360.,0.)
      Q1=(.0,.0)
      Q2=(.0,.0)
      IF(D1.LT.DKH)GO TO 200
      P1=(.0,.0)
      P2=CMPLX(.5*PSI/360.,0.)
      IF(D2.LT.DKH)GO TO 200
      SDK=SIN(DK)
      P1=(.0,.0)
      P2=(.0,.0)
      CBET=(X2-X1)/DK
      SBET=(Y2-Y1)/DK
      XA=(XS-X1)*CBET+(YS-Y1)*SBET
      YA=-(XS-X1)*SBET+(YS-Y1)*CBET
      X=XA
      Y=YA
      YSQ=Y**2
      RMIN=ABS(Y)
      IF(X.LT.C.)RMIN=SQRT(X*X+YSQ)
      IF(X.GT.DK)RMIN=SQRT((X-DK)**2+YSQ)
      FNT=1+(4*INT)/10
      ISS=FNT*DK/RMIN
      IF(ISS.LT.2)ISS=2
      FIT=ISS
      DS=DK/FIT
      XP=DS/2.
      DO 100 I=1,ISS
      DELX=X-XP
      RK=SQRT(DELX**2+YSQ)
      SPH=Y/RK
      S1=SIN(DK-XP)
      S2=SIN(XP)
      CALL HANK(RK,H0,H1,2)
      P1=P1+S1*H1*SPH
      P2=P2+S2*H1*SPH
      Q1=Q1+S1*H0
      Q2=Q2+S2*H0
      XP=XP+DS
  100 CONTINUE
      CST=(.0,1.)*DS/(4.*SDK)
      P1=CST*P1
      P2=CST*P2
      CNT=-DS/(4.*ETA*SDK)
      Q1=CNT*Q1
      Q2=CNT*Q2
  200 CONTINUE
      RETURN
      END
```

Fig. 39. Subroutine CMLS.

APPENDIX XIII
Subroutine VFF

VFF is listed in Fig. 40. In antenna problems (options 1, 2 and 3) and bistatic scattering (option 4 with INC = 0), VFF calculates the magnetic field HZT in the far-zone and the GAIN or the echo width EWL. In these cases, the current distribution CJ(I) on the cylinder is already known. VFF calls CFF to obtain the far-field from each strip on the cylinder. HJJ(I) and HMM(I) denote the fields from the electric and magnetic mode currents, respectively, of mode I. HZS is the field generated by the currents on the cylinder, HZM is the field of the magnetic line source in option 3, and HZT is the sum of these.

In backscattering problems (option 4 with INC = 1), VFF generates the excitation column which is related to HJJ(I) by the reciprocity theorem. Then VFF calls CROUT to obtain the current distribution CJ(I) and calculates the extinction cross-section ECS, the backscattered field and the echo width.

```
      SUBROUTINE VFF(IA,IB,INC,IDM,ISYM,IWR,I1,I2,I3,I12,LOP,MD,N,ND,NM,
     2C,CJ,D,EWL,G,GAIN,HJJ,HMM,HZS,HZT,PH,ECS,VJ,X,Y,XS,YS,ZS)
      COMPLEX COT,DOT,HJ1,HJ2,HM1,HM2,HZM,HZS,HZT,ZS
      COMPLEX CJ(IDM),HJJ(IDM),HMM(IDM),C(IDM,IDM),VJ(IDM)
      DIMENSION IA(IDM),IB(IDM),I1(IDM),I2(IDM),I3(IDM),MD(IDM,5)
      DIMENSION ND(IDM),X(IDM),Y(IDM),D(IDM)
      DATA ETA,TP/376.727,6.28318/
      COT=1.414214*ETA*CMPLX(1.,-1.)
      IF(ISYM.NE.0)DOT=COT*CONJG(ZS)/ZS
      ECS=.0
      PHR=.0174533*PH
      CPH=COS(PHR)
      SPH=SIN(PHR)
      DO 232 I=1,N
      HJJ(I)=(.0,.0)
  232 HMM(I)=(.0,.0)
      DO 250 K=1,NM
      KA=IA(K)
      KB=IB(K)
      CALL CFF(X(KA),Y(KA),X(KB),Y(KB),D(K)
     2,CPH,SPH,ZS,HJ1,HJ2,HM1,HM2)
      NDK=ND(K)
      DO 240 II=1,NDK
      I=MD(K,II)
      FI=1.
      IF(KB.EQ.I2(I))GO TO 236
      IF(KB.EQ.I1(I))FI=-1.
      HJJ(I)=HJJ(I)+FI*HJ1
      HMM(I)=HMM(I)+FI*HM1
      GO TO 240
  236 IF(KA.EQ.I3(I))FI=-1.
      HJJ(I)=HJJ(I)+FI*HJ2
      HMM(I)=HMM(I)+FI*HM2
  240 CONTINUE
  250 CONTINUE
      IF(INC.LE.0)GO TO 270
      DO 260 I=1,N
      CJ(I)=COT*HJJ(I)
      VJ(I)=CJ(I)
  260 IF(ISYM.NE.0)VJ(I)=VJ(I)-DOT*HMM(I)
      CALL CROUT(C,CJ,N,IDM,ISYM,IWR,I12)
      I12=2
      DO 265 I=1,N
  265 ECS=ECS+REAL(VJ(I)*CONJG(CJ(I)))
      ECS=ECS/ETA
  270 HZS=(.0,.0)
      DO 360 I=1,N
  360 HZS=HZS+CJ(I)*(HJJ(I)+HMM(I))
      HAB=CABS(HZS)
      IF(LOP.EQ.4)EWL=TP*HAB*HAB
      HZT=HZS
      IF(LOP.NE.3)GO TO 400
      PSI=XS*CPH+YS*SPH
      HZM=CMPLX(COS(PSI),SIN(PSI))
      HZM=-(1.,1.)*HZM/(2.*1.414214*ETA)
      HZT=HZS+HZM
  400 HAB=CABS(HZT)
      IF(LOP.LT.4)GAIN=TP*ETA*HAB*HAB/G
      RETURN
      END
```

Fig. 40. Subroutine VFF.

APPENDIX XIV
Subroutine CFF

CFF, listed in Fig. 41, calculates the far-zone field of a strip monopole. The endpoints of the monopole are at (XA,YA) and (XB,YB), and DK is the length. CPH and SPH denote $\cos\phi$ and $\sin\phi$. HJ1 and HJ2 are the far-field contributions from the electric mode currents with terminals at (XA,YA) and (XB,YB) respectively. Similarly HM1 and HM2 are the fields of the magnetic mode currents. This subroutine uses Eqs. (44) through (57).

```
      SUBROUTINE CFF(XA,YA,XB,YB,DK,CPH,SPH,ZS,HJ1,HJ2,HM1,HM2)
      COMPLEX EJA,EJB,CST,ZS,HJ1,HJ2,HM1,HM2
      DATA ETA,PI/376.727,3.14159/
      CA=(XB-XA)/DK
      CB=(YB-YA)/DK
      G=CA*CPH+CB*SPH
      P=CB*CPH-CA*SPH
      GK=P**2
      A=XA*CPH+YA*SPH
      B=XB*CPH+YB*SPH
      EJA=CMPLX(COS(A),SIN(A))
      EJB=CMPLX(COS(B),SIN(B))
      SDK=SIN(DK)
      CDK=COS(DK)
      IF(GK.LT..001)GO TO 250
      CST=CMPLX(1.,1.)/(4.*PI*SDK*1.414214*GK)
      HM1=CST*(EJA*CMPLX(CDK,G*SDK)-EJB)
      HM2=CST*(EJB*CMPLX(CDK,-G*SDK)-EJA)
      GO TO 300
  250 CST=CMPLX(-1.,1.)/(8.*PI*1.414214*SDK)
      IF(G.LT.0.)GO TO 280
      HM1=CST*(DK*EJB-SDK*EJA)
      HM2=CST*(SDK*EJB-DK*EJA)
      GO TO 300
  280 HM1=CST*(SDK*EJA-DK*EJB)
      HM2=CST*(DK*EJA-SDK*EJB)
  300 HJ1=P*HM1
      HJ2=P*HM2
      HM1=-ZS*HM1/ETA
      HM2=-ZS*HM2/ETA
      RETURN
      END
```

Fig. 41. Subroutine CFF.

APPENDIX XV
Subroutine CSURF

CSURF, listed in Fig. 42, calculates the surface impedance ZS of a plane conducting slab for normal incidence. FMC denotes the frequency in MHz. The conductivity of the slab material in megamhos per meter is CMM. The slab thickness is t and TK denotes kt.

```
      SUBROUTINE CSURF(CMM,FMC,TK,ZS)
      COMPLEX ETA,R,ZS,ETBT
      DATA E,ETA0,TP,U/8.85433E-12,376.727,6.28318,12.5664E-7/
      ALPH=SQRT(TP*FMC*U*CMM/2.)*1.E6
      SQT=SQRT(TP*FMC*U/(2.*CMM))
      ETA=CMPLX(SQT,SQT)
      TAT=2.*TK*SQRT(CMM/(2.*E*TP*FMC))
      ZS=ETA
      IF(TAT.GT.60.)GO TO 100
      ETAT=EXP(-TAT)
      ETBT=CMPLX(COS(TAT),-SIN(TAT))
      R=ETAT*ETBT*(ETA0-ETA)/(ETA0+ETA)
      ZS=ETA*(1.+R)/(1.-R)
  100 CONTINUE
      RETURN
      END
```

Fig. 42. Subroutine CSURF.